Geochemical Perspectives Letters

Light calcium isotope anomaly in the Pitcairn mantle plume: a signal of pyroxenite melting

Y. Wang[1], Y.-S. He[1*], O. Nebel[2], J.D. Woodhead[3]

OPEN ACCESS

https://doi.org/10.7185/geochemlet.2613

Abstract

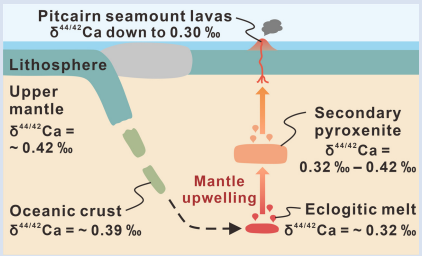

The light calcium (Ca) isotope anomaly observed in ocean island basalts (OIBs) compared to mid-ocean ridge lavas has typically been attributed to recycling of carbonate-bearing sediments, partial melting of garnet-rich lithologies or a combination of both. This study presents Ca isotopic data for lavas from Pitcairn Island and nearby seamounts, yielding a $\delta^{44/42}$Ca variation (0.30 ± 0.02 ‰ to 0.40 ± 0.02 ‰) similar to that found in global OIBs. This $\delta^{44/42}$Ca variation cannot be attributed to post-eruption alteration, magmatic differentiation or recycling of carbonate-bearing sediments. Instead, correlations of $\delta^{44/42}$Ca with Sr/Nd and Eu/Eu* suggest that the light Ca isotope anomaly in Pitcairn lavas most likely reflects derivation from a pyroxenite source akin to the lower part of the recycled oceanic crust. Modelling suggests that the low $\delta^{44/42}$Ca end member can be explained by multiple-stage pyroxenite melting without requiring recycled carbonate-bearing sediments, offering new insights into using Ca isotopes to trace crust-mantle interactions.

Received 1 April 2025 | Accepted 11 March 2026 | Published 17 April 2026

Introduction

Ocean island basalts (OIBs), as melting products of upwelling mantle plumes, provide critical insights into mantle heterogeneity. In recent decades, calcium (Ca) isotopes have shown great potential for tracing recycled carbonates and lithological diversity in the deep mantle. A light Ca isotope anomaly was first observed in Hawaiian basalts and was attributed to recycled ancient carbonates, which have significantly higher CaO contents and lighter Ca isotopic compositions than the upper mantle (Huang *et al.*, 2011). Similar light Ca isotope anomalies identified in mantle-derived magmas have been suggested to be related to source hybridisation by subducted carbonates (Liu *et al.*, 2017; He *et al.*, 2023; Wang *et al.*, 2023), and have now been observed in many more hotspots such as Pitcairn, Tristan da Cunha, and Kerguelen (enriched mantle-1, EM-1), Samoa, Society (enriched mantle-2, EM-2) and the Canaries (high-^{238}U/^{204}Pb, HIMU), confirming substantial Ca isotope variations as a common phenomenon among global OIBs (Eriksen and Jacobsen, 2022; Eriksen *et al.*, 2024). A number of recent studies favour a lithological control on Ca isotopic composition and invoke isotopic fractionation during melting of garnet-rich pyroxenites (Eriksen and Jacobsen, 2022; Eriksen *et al.*, 2024), as garnet is rich in both Ca and heavy Ca isotopes compared with other mantle minerals (Wang *et al.*, 2019; Antonelli *et al.*, 2021a). Nevertheless, independent evidence (including carbonatitic inclusions in olivine phenocrysts, the presence of associated carbonatite, trace element patterns typical of carbonatitic metasomatism in the source, enriched Sr-Nd-Pb isotopic compositions, as well as light Mg and heavy Zn isotope anomalies) suggests that recycled components, possibly containing carbonates, are prevalent in the sources of OIBs with light Ca isotope compositions (*e.g.*, Eisele *et al.*, 2002; Castillo, 2015; Wang *et al.*, 2018; Zhang *et al.*, 2022). Therefore, it remains a subject of debate as to what extent recycling of isotopically light Ca crustal components (*e.g.*, carbonates) and isotopic fractionation during melting of garnet-bearing lithologies contribute to Ca isotope variations in OIBs.

Here we examine this puzzle by measuring a suite of well-characterised lavas from the Pitcairn mantle plume, which exhibits significant chemical and isotopic variability ranging from a typical EM-1 end member to a markedly depleted one (Woodhead and McCulloch, 1989; Woodhead and Devey, 1993). The EM-1 component is typically defined by high ^{87}Sr/^{86}Sr, low ^{143}Nd/^{144}Nd and unradiogenic Pb isotopic compositions (Zindler and Hart, 1986). This sample diversity in a single plume enables us to distinguish between the contributions of recycled carbonate sediments and isotopic fractionation during partial melting to the Ca isotope variation. Our results identify a Ca isotope variation almost as large as that found in global OIBs. Combined with published data, we show that the isotopically light end member of Pitcairn lavas is akin to recycling of the lower (gabbroic) oceanic crust and suggest a dominant role of isotopic fractionation during multi-stage pyroxenite melting in its source (*e.g.*, Nebel *et al.*, 2019).

1. State Key Laboratory of Geological Processes and Mineral Resources, China University of Geosciences, Beijing 100083, China
2. GEOMAR Helmholtz Centre for Oceanic Research, 24148 Kiel, Germany
3. School of Geography, Earth and Atmospheric Sciences, University of Melbourne, Parkville, VIC 3010, Australia
* Corresponding author (email: heys@cugb.edu.cn)

Samples and Analytical Method

The samples measured in this study include five Tedside shield-building basalts and three post-erosional basalts from Pitcairn Island (Woodhead and McCulloch, 1989) and seven seamount lavas from Volcano 2 erupted on the adjacent ocean floor (Woodhead and Devey, 1993). Phenocrysts primarily consist of olivine, clinopyroxene, and plagioclase. The CaO-MgO diagram suggests that olivine was the dominant liquidus phase during early differentiation (*e.g.*, MgO ≥ 3.8 wt. %), transitioning to clinopyroxene dominance in more evolved lavas (Fig. S-1). Al_2O_3 behaves as an incompatible element until MgO content drops below ~1 wt. % (Fig. S-1), suggesting limited plagioclase control on the samples analysed here (*i.e.* all have MgO ≥ 1.18 wt. %). Tedside samples are characterised by notably high $^{87}Sr/^{86}Sr$, low $^{143}Nd/^{144}Nd$ and low $^{206}Pb/^{204}Pb$ ratios, whereas the post-erosional and seamount samples exhibit variable degrees of depletion in Sr-Nd-Pb isotopic compositions, suggesting mixing between an enriched EM-1 component and a more depleted component (Fig. S-1; Woodhead and Devey, 1993; Eisele *et al.*, 2002).

Calcium isotope analyses followed He *et al.* (2017) and were performed at the Isotope Geochemistry Laboratory, China University of Geosciences, Beijing. Stable Ca isotopic compositions and radiogenic ^{40}Ca excesses/deficits are reported in δ and ε notations, respectively, relative to SRM915a, with $\varepsilon^{40/44}Ca$ calculated from $\delta^{44/40}Ca$ and $\delta^{44/42}Ca$ using the exponential law (Farkaš *et al.*, 2011; He *et al.*, 2017). To minimise possible effects of radiogenic ^{40}Ca, we discuss stable Ca isotopes primarily in terms of $\delta^{44/42}Ca$. Analytical procedures and full datasets for samples and reference materials are given in the Supplementary Information and Tables S-1 and S-2.

Results

The Pitcairn samples exhibit a $\delta^{44/42}Ca$ range from a mid-ocean ridge basalt (MORB)-like value of 0.40 ± 0.02 ‰ to as low as 0.30 ± 0.03 ‰ ($\delta^{44/40}Ca = 0.68 \pm 0.08$ ‰ to 0.84 ± 0.04 ‰; Fig. 1; Table S-1). Five enriched Tedside samples, characterised by high $^{87}Sr/^{86}Sr$ and low $^{143}Nd/^{144}Nd$ ratios indicative of EM-1 mantle components (Woodhead and McCulloch, 1989), have a mean $\delta^{44/42}Ca$ value of 0.37 ± 0.02 ‰ (2 s.d., $n = 5$). No systematic correlations are observed between $\delta^{44/42}Ca$ and Sr-Nd-Pb isotopic ratios or differentiation indices such as MgO and CaO (Figs. S-2 and S-3; Table S-3). $\varepsilon^{40/44}Ca$ values range from −1.3 ± 0.5 to +0.4 ± 0.3 (Table S-1). $\varepsilon^{40/44}Ca$ values in the Tedside samples are systematically higher than the BSE value (*e.g.*, −1.2; Antonelli *et al.*, 2021b), likely reflecting the contribution of a recycled component within the Pitcairn mantle plume (Fig. S-4). Detailed discussion of these results is provided in the Supplementary Information, and our subsequent discussion focuses on stable Ca isotopes ($\delta^{44/42}Ca$).

Role of post-extraction processes

All Pitcairn samples analysed in this study are fresh (LOI < 0.5 wt. %), indicating negligible post-eruption alteration. However, these samples have undergone varying degrees of magmatic differentiation. During early differentiation, olivine was the dominant crystallising phase (Fig. S-1), which likely had little effect on the $\delta^{44/42}Ca$ values of samples with MgO ≥ 3.8 wt. % (Fig. S-4). Three more-evolved lavas (P1, 45DS1, and 51DS4), with MgO < 3.8 wt. %, underwent substantial clinopyroxene crystallisation. Because clinopyroxene has slightly higher $\delta^{44/42}Ca$ values than its co-existing melt (Zhang *et al.*, 2018; Eriksen and Jacobsen, 2022), its crystallisation may have led to a minor decrease in the $\delta^{44/42}Ca$ value of the remaining melt (Zhang *et al.*, 2018; Wang *et al.*, 2023). Nevertheless, relatively heavy $\delta^{44/42}Ca$ values are observed in these three evolved samples, suggesting slightly higher primary $\delta^{44/42}Ca$ values than measured. Negative correlations of $\delta^{44/42}Ca$ with Sr/Nd and Eu/Eu* may suggest a role for plagioclase crystallisation (Fig. 2; Table S-4); however, this can be ruled out by the incompatible behaviour of Al_2O_3 during differentiation of the Pitcairn lavas measured here (Fig. S-1). Thus, the decreased $\delta^{44/42}Ca$ values in Pitcairn samples are not a consequence of magmatic differentiation but most likely reflects primary source characteristics.

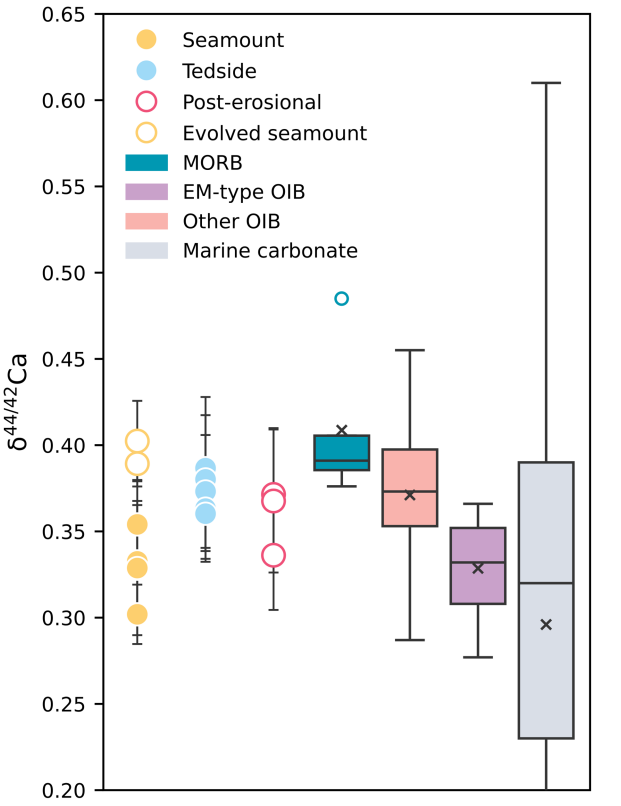

Figure 1 $\delta^{44/42}Ca$ for Pitcairn basalts. MORB, EM-type OIBs (EM-1/EM-2; enriched radiogenic isotopes), other OIBs and marine carbonates are shown for comparison. MORB and OIB data are from Eriksen and Jacobsen (2022) and Eriksen *et al.* (2024); marine carbonate data are from Fantle and Tipper (2014).

Origin of light Ca isotope anomaly among Pitcairn lavas

Low MgO (<3.8 wt. %) samples may be at risk of having experienced significant fractional crystallisation (Fig. S-1) and three post-erosional samples (erupted ~0.3 Myr after Tedside) do not follow the main Sr-Nd isotopic trend (Woodhead and McCulloch, 1989). We therefore focus our discussion of the origin of the Pitcairn source primarily on the ten Tedside and seamount samples with MgO ≥ 3.8 wt. % in order to minimise the influence of late stage processes and source heterogeneity, although these samples define the same trends in $\delta^{44/42}Ca$ *versus* Sr/Nd and Eu/Eu* plots. Accordingly, because (i) the early crystallising (MgO ≥ 3.8 wt. %) assemblage is dominated by olivine ± clinopyroxene with no plagioclase involvement (Fig. S-1) and (ii) melting occurred at garnet-facies pressures where plagioclase is unstable, the observed Sr/Nd and Eu/Eu* variations

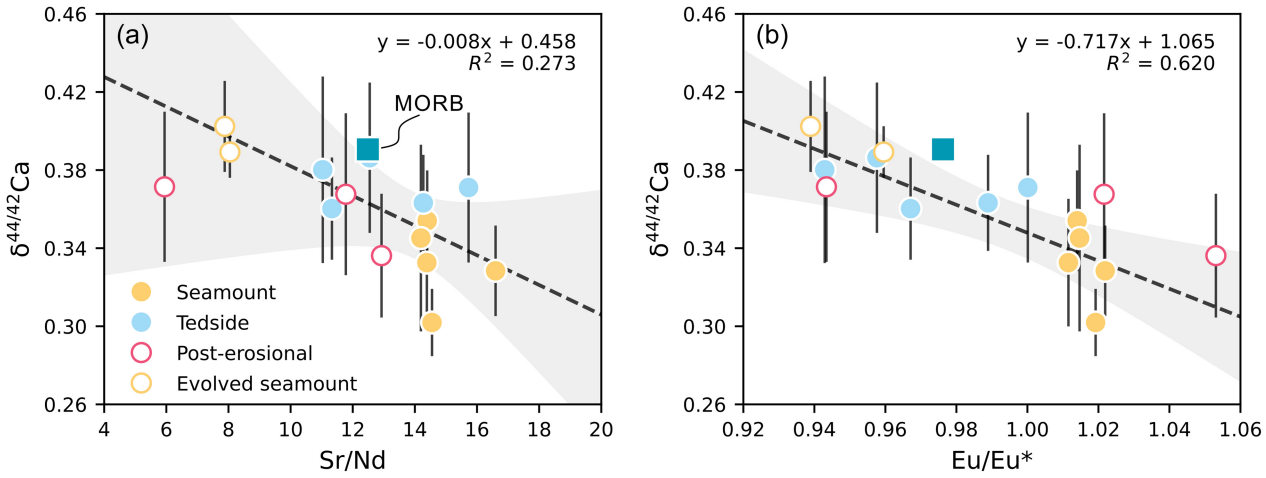

Figure 2 $\delta^{44/42}$Ca *versus* **(a)** Sr/Nb and **(b)** Eu/Eu* for Pitcairn basalts. Eu/Eu* = $Eu_N/(Sm_N \times Gd_N)^{0.5}$, where the subscript 'N' denotes chondrite-normalised values (Sun and McDonough, 1989). Trace element data are from Woodhead and McCulloch (1989) and Woodhead and Devey (1993). Filled symbols, Tedside + seamount samples with MgO ≥ 3.8 wt. % (used in fits); open symbols, post-erosional and evolved samples with MgO < 3.8 wt. % (excluded). Black line, linear regression fit to Tedside + seamount samples (MgO ≥ 3.8 wt. %); grey band, 95 % CI. MORB $\delta^{44/42}$Ca values are from Eriksen and Jacobsen (2022). Pitcairn trace elements are corrected for olivine accumulation following Nebel *et al.* (2019) (Table S-4), except for those with MgO < 3.8 wt. %, for which an effective clinopyroxene correction is unavailable.

record source metasomatism by at least two groups of crustal components, rather than magmatic processes. One group has sub-chondritic Sr/Nd and Eu/Eu* < 1, akin to sediments and the differentiated upper oceanic crust that has undergone plagioclase crystallisation. The other has high Sr/Nd and Eu/Eu* > 1, similar to gabbros in the lower oceanic crust that have experienced plagioclase accumulation (Fig. S-5). The involvement of surface crustal materials in the Pitcairn plume source has been independently inferred from low δ^{26}Mg values (Wang *et al.*, 2018) and mass independent Hg isotope fractionations (Moynier *et al.*, 2021). Nevertheless, samples with the lowest Sr/Nd and Eu/Eu* values and enriched radiogenic isotopes display MORB-like $\delta^{44/42}$Ca values, whereas light Ca isotope anomalies are observed in the depleted end member (Fig. 2; Fig. S-2). These puzzling trends are inconsistent with incorporation of low $\delta^{44/42}$Ca recycled sediments, and require an alternative mechanism to explain the low $\delta^{44/42}$Ca values in Pitcairn OIBs.

Unlike surface crustal materials with fractionated $\delta^{44/42}$Ca values, the gabbroic lower oceanic crust has a mean $\delta^{44/42}$Ca value comparable to that of the upper mantle (Fig. S-6). Therefore, the low $\delta^{44/42}$Ca magma end member cannot result from simple binary mixing between gabbroic lower oceanic crust and upper mantle but instead reflects Ca isotope fractionation during mantle metasomatism and late partial melting. Partial melting of pyroxenites with abundant residual garnet provides a plausible mechanism for generating melts with low $\delta^{44/42}$Ca values (Wang *et al.*, 2019, 2023; Eriksen and Jacobsen, 2022).

To quantitatively evaluate isotopic fractionation during partial melting, we perform incremental non-modal batch melting modelling for various mantle lithologies, including spinel- and garnet-bearing peridotite, recycled MORB (*i.e.* eclogite), and secondary pyroxenites generated by reaction between eclogite-derived melts and peridotite. The initial $\delta^{44/42}$Ca values for mantle peridotite and eclogite were set at 0.42 ‰ (Kang *et al.*, 2017) and 0.39 ‰ (Eriksen and Jacobsen, 2022), respectively. Melting conditions and modes were based on relevant experimental studies. Details of the modelling calculation are provided in the Supplementary Information and Tables S-5 to S-10.

Our results suggest that Ca isotope fractionation is limited during partial melting of peridotites and secondary pyroxenites in which garnet, if present, is less abundant (Fig. 3a), mainly due to the buffering effect of Ca-rich clinopyroxene, which has only slightly heavier Ca isotopic compositions than co-existing melts (Zhang *et al.*, 2018; Eriksen and Jacobsen, 2022). Partial melting of either garnet peridotite or secondary pyroxenite with a mantle-like $\delta^{44/42}$Ca value can account for the heavy $\delta^{44/42}$Ca magma end member but fails to explain both the lightest $\delta^{44/42}$Ca values and the steep slope of Pitcairn basalts in $\delta^{44/42}$Ca *versus* $(Dy/Yb)_N$ space (Fig. 3a). The involvement of abundant partial melts of recycled oceanic crust has been suggested for the source of the isotopically light seamount lavas (Woodhead and Devey, 1993; Eisele *et al.*, 2002; Delavault *et al.*, 2016). Partial melting of eclogite at high pressure (*e.g.*, 3–5 GPa; Sobolev *et al.*, 2005) in the deep mantle can generate melts with much lower $\delta^{44/42}$Ca values around 0.31 ‰, as garnet is abundant in the residua and minimally involved in the melting process (Table S-7). However, the proportion of eclogite-derived melts directly contributing to OIBs is likely limited (Sobolev *et al.*, 2007), and modelling calculations show that the trace element compositions (*e.g.*, $(Dy/Yb)_N$) do not match the characteristics of Pitcairn basalts (Fig. 3a). Instead, hybridisation of peridotite with high proportions of high pressure eclogite-derived melts (HPEMs) can produce secondary pyroxenites with lower $\delta^{44/42}$Ca and $(Dy/Yb)_N$ values. For example, mixing peridotite and HPEM in a 1:1 ratio (similar to Koolau lavas in Hawaii; Sobolev *et al.*, 2005) yields a secondary pyroxenite with $\delta^{44/42}$Ca ≈ 0.34 ‰ and $(Dy/Yb)_N \approx 1.29$ (Table S-8). High degrees of partial melting of such lithologies can resemble both the $\delta^{44/42}$Ca and $(Dy/Yb)_N$ values of the low $\delta^{44/42}$Ca magma end member among Pitcairn lavas (Fig. 3a).

Olivine and whole-rock compositions also suggest the contribution of pyroxenite sources to Pitcairn lavas (*e.g.*, Delavault *et al.*, 2015; Garapić *et al.*, 2015). Pyroxenite in the source of Pitcairn lavas with MORB-like $\delta^{44/42}$Ca values may form either from low HPEM proportions (*e.g.*, ~5 %; Fig. 3) or by mechanical mixing between recycled eclogite and mantle peridotite (Fig. S-6c). Our model illustrates a simple binary mixing scenario between melts derived from two secondary pyroxenites that differ in HPEM proportion. The MORB-like $\delta^{44/42}$Ca end member is derived from a secondary pyroxenite formed by ~5 % HPEM. To reproduce the enriched $^{87}Sr/^{86}Sr$ of the Tedside

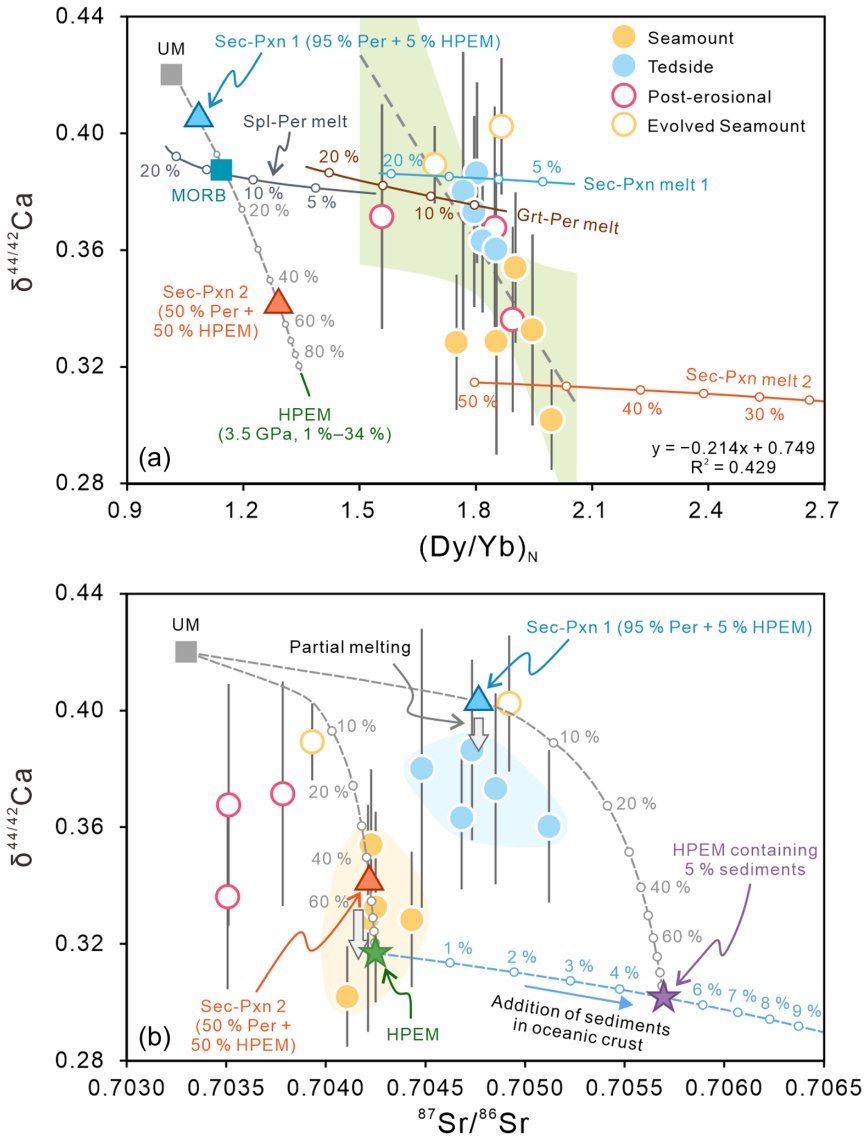

Figure 3 Model illustrating the origin of Ca isotope variations in the Pitcairn mantle plume. $\delta^{44/42}$Ca *versus* **(a)** $(Dy/Yb)_N$ and **(b)** $^{87}Sr/^{86}Sr$. Symbols and regression band are as in Figure 2. In **(a)**, grey and brown solid curves represent partial melting of spinel- and garnet-bearing peridotite, respectively, whereas blue and orange curves represent melting of two secondary pyroxenite end members. In **(b)**, the blue dashed line illustrates the effects of adding carbonate-bearing sediments to recycled oceanic crust to generate HPEM. In both panels, grey dashed lines represent the formation of secondary pyroxenites through interaction between HPEM and ambient peridotite at different proportions; blue and orange triangles indicate the resulting secondary pyroxenite end members. Abbreviations: Spl-Per, spinel peridotite; Grt-Per, garnet peridotite; Sec-Pxn, secondary pyroxenite; HPEM, high pressure eclogite-derived melt; UM, upper mantle. Modelling details are provided in the Supplementary Information and Tables S-5–S-10.

lavas, ~5 % carbonate-bearing sediments are included in the recycled oceanic crust generating the HPEM component. Because sediments contain much higher Sr concentrations than oceanic crust, this addition strongly influences $^{87}Sr/^{86}Sr$ but has only a negligible effect on $\delta^{44/42}$Ca (Fig. 3b; see the Supplementary Information). In contrast, the low $\delta^{44/42}$Ca end member, derived from a secondary pyroxenite containing ~50 % HPEM, displays higher Eu/Eu* and lower $^{87}Sr/^{86}Sr$, pointing to recycled lower oceanic crust with less sediments (Fig. 3b). Binary mixing between melts from these two pyroxenites reproduces the observed $\delta^{44/42}$Ca variations with trace element ratios (Figs. 2 and 3a) and radiogenic isotope ratios (Fig. 3b). Accordingly, secondary pyroxenite formed through interaction between HPEM and ambient mantle peridotite is likely a key control on the Ca isotopic variations of Pitcairn basalts. Whereas carbonatite melting can lower $\delta^{44/42}$Ca values in principle (Antonelli *et al.*, 2023), our Pitcairn lavas show no geochemical evidence for carbonatite involvement (*e.g.*, low CaO/Al_2O_3 and Ba/Nb, Fig. S-7), and the observed $\delta^{44/42}$Ca variations are fully explained by multi-stage melting and mixing among secondary pyroxenite melts at ~1400 °C. We therefore consider any carbonatite contribution to be minor at most and not required here.

Our study reaffirms the role of pyroxenite melting at pressures >3.0 GPa in generating metasomatic agents with low $\delta^{44/42}$Ca values but moderate $(Dy/Yb)_N$ ratios (Fig. 3). The Tedside basalts, representing the EM-1 end member, display higher $\delta^{44/42}$Ca values of 0.36–0.39 ‰, whereas the depleted seamount basalts exhibit notably lower $\delta^{44/42}$Ca values of 0.30–0.35 ‰. The lightest $\delta^{44/42}$Ca end member among the Pitcairn lavas shows geochemical signatures associated with the recycling of lower oceanic crust, which typically contains little

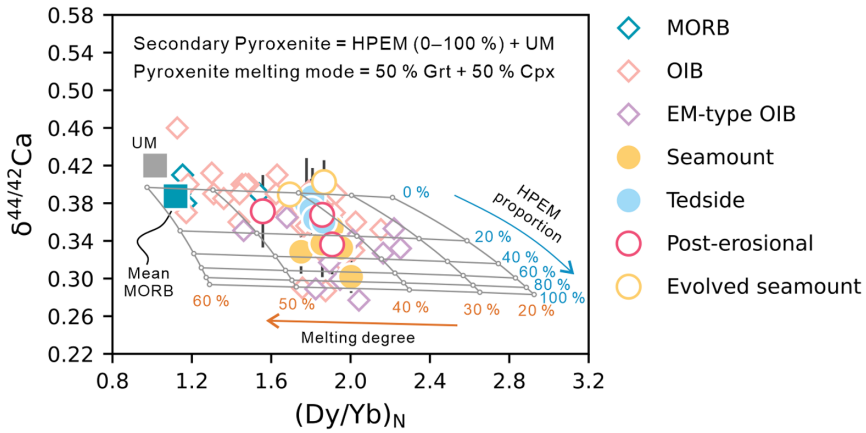

Figure 4 $\delta^{44/42}$Ca *versus* $(Dy/Yb)_N$ for global OIBs. Literature data are from Eriksen and Jacobsen (2022) and Eriksen et al. (2024). Symbols are as in Figure 2. Upper mantle and MORB $\delta^{44/42}$Ca references are as in Figure 3. The black grid represents our modelling of REEs and $\delta^{44/42}$Ca; see the Supplementary Information for details.

sediment and altered carbonate. Negative correlations with Sr/Nd and Eu/Eu* further indicate that this isotopically light Ca end member can be attributed to the recycling of lower gabbroic oceanic crust and isotopic fractionation during multi-stage pyroxenite melting. This study demonstrates that the lightest $\delta^{44/42}$Ca OIBs can be generated by partial melting of a mantle source involving a pyroxenitic component in the Pitcairn plume, rather than by contributions from recycled carbonate-bearing sediments. More broadly, the Pitcairn trend in $\delta^{44/42}$Ca *versus* $(Dy/Yb)_N$ space closely resembles the compositional range of global OIBs at the high $(Dy/Yb)_N$ end (Fig. 4), suggesting that similar processes involving HPEM and partial melting of its derivative secondary pyroxenite may also contribute to the origin of low $\delta^{44/42}$Ca signatures in other OIBs (Eriksen and Jacobsen, 2022; Eriksen *et al.*, 2024). This implies that interpretations of low $\delta^{44/42}$Ca signatures in OIBs as direct evidence for recycled carbonate-bearing sediments should be approached with caution (*e.g.*, Wang *et al.*, 2023).

Acknowledgements

We sincerely thank editor Helen Williams, reviewer Zack Eriksen, and an anonymous reviewer for their insightful comments that greatly improved this manuscript. This work was financially supported by the National Key Research and Development Project of China (2023YFF0804100), the National Natural Science Foundation of China (Nos. 42288201, 42103010, and 42122019), Fundamental Research Funds for the Central Universities (2652023001, 2652023005), and State Key Laboratory of Geological Processes and Mineral Resources. ON acknowledges support by the DFG (Heisenberg grant no. 533104367).

Editor: Helen Williams

Additional Information

Supplementary Information accompanies this letter at https://www.geochemicalperspectivesletters.org/article2613.

Cite this letter as: Wang, Y., He, Y.-S., Nebel, O., Woodhead, J.D. (2026) Light calcium isotope anomaly in the Pitcairn mantle plume: a signal of pyroxenite melting. *Geochem. Persp. Let.* 39, 54–59. https://doi.org/10.7185/geochemlet.2613

References

Antonelli, M.A., Kendrick, J., Yakymchuk, C., Guitreau, M., Mittal, T., Moynier, F. (2021a) Calcium isotope evidence for early Archaean carbonates and subduction of oceanic crust. *Nature Communications* 12, 2534. https://doi.org/10.1038/s41467-021-22748-2

Antonelli, M.A., DePaolo, D.J., Christensen, J.N., Wotzlaw, J.-F., Pester, N.J., Bachmann, O. (2021b) Radiogenic ^{40}Ca in Seawater: Implications for Modern and Ancient Ca Cycles. *ACS Earth and Space Chemistry* 5, 2481–2492. https://doi.org/10.1021/acsearthspacechem.1c00179

Antonelli, M.A., Sartori, G., Giuliani, A., Schauble, E.A., Hoffmann, J., Schmidt, M.W. (2023) Calcium isotope fractionation during melt immiscibility and carbonatite petrogenesis. *Geochemical Perspectives Letters* 28, 13–19. https://doi.org/10.7185/geochemlet.2338

Castillo, P.R. (2015) The recycling of marine carbonates and sources of HIMU and FOZO ocean island basalts. *Lithos* 216–217, 254–263. https://doi.org/10.1016/j.lithos.2014.12.005

Delavault, H., Chauvel, C., Sobolev, A., Batanova, V. (2015) Combined petrological, geochemical and isotopic modeling of a plume source: Example of Gambier Island, Pitcairn chain. *Earth and Planetary Science Letters* 426, 23–35. https://doi.org/10.1016/j.epsl.2015.06.013

Delavault, H., Chauvel, C., Thomassot, E., Devey, C.W., Dazas, B. (2016) Sulfur and lead isotopic evidence of relic Archean sediments in the Pitcairn mantle plume. *Proceedings of the National Academy of Sciences* 113, 12952–12956. https://doi.org/10.1073/pnas.1523805113

Eisele, J., Sharma, M., Galer, S.J.G., Blichert-Toft, J., Devey, C.W., Hofmann, A.W. (2002) The role of sediment recycling in EM-1 inferred from Os, Pb, Hf, Nd, Sr isotope and trace element systematics of the Pitcairn hotspot. *Earth and Planetary Science Letters* 196, 197–212. https://doi.org/10.1016/S0012-821X(01)00601-X

Eriksen, Z.T., Jacobsen, S.B. (2022) Calcium isotope constraints on OIB and MORB petrogenesis: The importance of melt mixing. *Earth and Planetary Science Letters* 593, 117665. https://doi.org/10.1016/j.epsl.2022.117665

Eriksen, Z.T., Jacobsen, S.B., Day, J.M.D., White, W.M. (2024) Calcium isotope variability among ocean islands reveals the physical and lithological controls on mantle partial melting. *Geochimica et Cosmochimica Acta* 373, 326–341 https://doi.org/10.1016/j.gca.2024.02.011

Fantle, M.S., Tipper, E.T. (2014) Calcium isotopes in the global biogeochemical Ca cycle: Implications for development of a Ca isotope proxy. *Earth-Science Reviews* 129, 148–177. https://doi.org/10.1016/j.earscirev.2013.10.004

Farkaš, J., Déjeant, A., Novák, M., Jacobsen, S.B. (2011) Calcium isotope constraints on the uptake and sources of Ca^{2+} in a base-poor forest: A new concept of combining stable ($\delta^{44/42}Ca$) and radiogenic (εCa) signals. *Geochimica et Cosmochimica Acta* 75, 7031–7046. https://doi.org/10.1016/j.gca.2011.09.021

Garapić, G., Jackson, M.G., Hauri, E.H., Hart, S.R., Farley, K.A., Blusztajn, J.S., Woodhead, J.D. (2015) A radiogenic isotopic (He-Sr-Nd-Pb-Os) study of lavas from the Pitcairn hotspot: Implications for the origin of EM-1 (enriched mantle 1). *Lithos* 228–229, 1–11. https://doi.org/10.1016/j.lithos.2015.04.010

He, Y., Wang, Y., Zhu, C., Huang, S., Li, S. (2017) Mass-Independent and Mass-Dependent Ca Isotopic Compositions of Thirteen Geological Reference Materials Measured by Thermal Ionisation Mass Spectrometry. *Geostandards and Geoanalytical Research* 41, 283–302. https://doi.org/10.1111/ggr.12153

He, D., Liu, Y., Moynier, F., Foley, S.F., Chen, C., Zhu, Y., Lü, X., Zhang, G., Zong, K. (2023) Tightly coupled Ca-Zn-Sr isotope co-variations in basalts caused by recycled calcium carbonate in the mantle source. *Chemical Geology* 637, 121678. https://doi.org/10.1016/j.chemgeo.2023.121678

Huang, S., Farkaš, J., Jacobsen, S.B. (2011) Stable calcium isotopic compositions of Hawaiian shield lavas: Evidence for recycling of ancient marine carbonates into the mantle. *Geochimica et Cosmochimica Acta* 75, 4987–4997. https://doi.org/10.1016/j.gca.2011.06.010

Kang, J.-T., Ionov, D.A., Liu, F., Zhang, C.-L., Golovin, A.V., Qin, L.-P., Zhang, Z.-F., Huang, F. (2017) Calcium isotopic fractionation in mantle peridotites by melting and metasomatism and Ca isotope composition of the Bulk Silicate Earth. *Earth and Planetary Science Letters* 474, 128–137. https://doi.org/10.1016/j.epsl.2017.05.035

Liu, F., Li, X., Wang, G., Liu, Y., Zhu, H., Kang, J., Huang, F., Sun, W., Xia, X., Zhang, Z. (2017) Marine Carbonate Component in the Mantle Beneath the Southeastern Tibetan Plateau: Evidence From Magnesium and Calcium Isotopes. *Journal of Geophysical Research: Solid Earth* 122, 9729–9744. https://doi.org/10.1002/2017JB014206

Moynier, F., Jackson, M.G., Zhang, K., Cai, H., Halldórsson, S.A., Pik, R., Day, J.M.D., Chen, J. (2021) The Mercury Isotopic Composition of Earth's Mantle and the Use of Mass Independently Fractionated Hg to Test for Recycled Crust. *Geophysical Research Letters* 48, e2021GL094301. https://doi.org/10.1029/2021GL094301

Nebel, O., Sossi, P.A., Bénard, A., Arculus, R.J., Yaxley, G.M., Woodhead, J.D., Davies, D.R., Ruttor, S. (2019) Reconciling petrological and isotopic mixing mechanisms in the Pitcairn mantle plume using stable Fe isotopes. *Earth and Planetary Science Letters* 521, 60–67. https://doi.org/10.1016/j.epsl.2019.05.037

Sobolev, A.V., Hofmann, A.W., Sobolev, S.V., Nikogosian, I.K. (2005) An olivine-free mantle source of Hawaiian shield basalts. *Nature* 434, 590–597. https://doi.org/10.1038/nature03411

Sobolev, A.V., Hofmann, A.W., Kuzmin, D.V., Yaxley, G.M., Arndt, N.T., *et al.* (2007) The Amount of Recycled Crust in Sources of Mantle-Derived Melts. *Science* 316, 412–417. https://doi.org/10.1126/science.1138113

Sun, S.-s., McDonough, W.F. (1989) Chemical and isotopic systematics of oceanic basalts: implications for mantle composition and processes. *Geological Society, London, Special Publications* 42, 313–345. https://doi.org/10.1144/GSL.SP.1989.042.01.19

Wang, X.-J., Chen, L.-H., Hofmann, A.W., Hanyu, T., Kawabata, H., *et al.* (2018) Recycled ancient ghost carbonate in the Pitcairn mantle plume. *Proceedings of the National Academy of Sciences* 115, 8682–8687. https://doi.org/10.1073/pnas.1719570115

Wang, Y., He, Y., Wu, H., Zhu, C., Huang, S., Huang, J. (2019) Calcium isotope fractionation during crustal melting and magma differentiation: Granitoid and mineral-pair perspectives. *Geochimica et Cosmochimica Acta* 259, 37–52. https://doi.org/10.1016/j.gca.2019.05.030

Wang, Y., Meng, X., He, Y., Huang, J., Lu, W.-N., Shi, Q., Ke, S., Tang, Y.-J., Huang, S., Li, S. (2023) Light calciumisotope anomaly observed in continental basaltic lavas: A mixed signal of recycled carbonate and fractionation during melting. *Lithos* 456–457, 107307. https://doi.org/10.1016/j.lithos.2023.107307

Woodhead, J.D., Devey, C.W. (1993) Geochemistry of the Pitcairn seamounts, I: source character and temporal trends. *Earth and Planetary Science Letters* 116, 81–99. https://doi.org/10.1016/0012-821X(93)90046-C

Woodhead, J.D., McCulloch, M.T. (1989) Ancient seafloor signals in Pitcairn Island lavas and evidence for large amplitude, small length-scale mantle heterogeneities. *Earth and Planetary Science Letters* 94, 257–273. https://doi.org/10.1016/0012-821X(89)90145-3

Zhang, H., Wang, Y., He, Y., Teng, F., Jacobsen, S.B., Helz, R.T., Marsh, B.D., Huang, S. (2018) No Measurable Calcium Isotopic Fractionation During Crystallization of Kilauea Iki Lava Lake. *Geochemistry, Geophysics, Geosystems* 19, 3128–3139. https://doi.org/10.1029/2018GC007506

Zhang, X.-Y, Chen, L.-H., Wang, X.-J., Hanyu, T., Hofmann, A.W., Komiya, T., Nakamura, K., Kato, Y., Zeng, G., Gou, W.-X., Li, W.-Q. (2022) Zinc isotopic evidence for recycled carbonate in the deep mantle. *Nature Communications* 13, 6085. https://doi.org/10.1038/s41467-022-33789-6

Zindler, A., Hart, S. (1986) Chemical Geodynamics. *Annual Reviews of Earth and Planetary Sciences* 14, 493–571. https://doi.org/10.1146/annurev.ea.14.050186.002425

Geochemical Perspectives Letters

Light calcium isotope anomaly in the Pitcairn mantle plume: a signal of pyroxenite melting

Y. Wang, Y.-S. He, O. Nebel, J.D. Woodhead

Supplementary Information

The Supplementary Information includes:

- 1. Ca Isotope Analysis Method
- 2. Radiogenic Ca Isotope Variation in Pitcairn Lavas
- 3. Modelling the Ca Isotope Composition of Melts in This Study
- Tables S-1 to S-10
- Figures S-1 to S-7
- Supplementary Information References

1. Ca Isotope Analysis Method

Calcium isotope analyses were performed at the Isotope Geochemistry Laboratory, China University of Geosciences, Beijing, following procedures detailed by He *et al.* (2017). Approximately 3 mg of powdered sample was dissolved in a concentrated HNO_3-HCl-HF mixture. One aliquot of the sample solutions, containing approximately 30 µg of Ca, was mixed with a ^{43}Ca-^{48}Ca double spike and then purified using AG50W-X12 resin (200–400 mesh, Bio-Rad). Isotope measurements were conducted using a Triton Plus thermal ionisation mass spectrometer (TIMS) equipped with customised L5 and H4 cups, allowing for static measurement of all Ca isotopes. Double Re filament assemblies were used, with approximately 5 µg of Ca loaded onto each evaporation filament. The ^{40}Ca signal intensity was approximately 15 V. Each analysis consisted of 120 cycles with an integration time of 16.776 s per cycle. Results are reported in δ notations relative to SRM915a, which was measured during each session:

$$\delta^{44/i}Ca\ (‰) = [(^{44}Ca/^{i}Ca)_{sample} / (^{44}Ca/^{i}Ca)_{SRM915a} - 1] \times 1000 \qquad \text{Eq. S-1}$$

where i represents 40 or 42. A secondary correction was applied using geological standard materials bracketing the unknown samples against their long-term values (Wang *et al.*, 2023). Radiogenic ^{40}Ca excess or deficit, expressed as ε values, was calculated from $\delta^{44/40}$Ca and $\delta^{44/42}$Ca values using the following equation:

$$\varepsilon^{40/44}\text{Ca} = (\delta^{44/42}\text{Ca} \times 2.0483 - \delta^{44/40}\text{Ca}) \times 10 \quad \text{Eq. S-2}$$

where the coefficient 2.0483 corresponds to the slope of mass-dependent fractionation in the exponential law (Farkaš *et al.*, 2011; He *et al.*, 2017). Multiple measurements were performed for each sample to improve precision, with means and 2 s.e. values reported (Table S-1). The long-term precision was ±0.03 ‰ and ±0.6 ε for $\delta^{44/42}$Ca and $\varepsilon^{40/44}$Ca, with each sample typically measured eight times (He *et al.*, 2017; Wang *et al.*, 2023). Measurements of reference materials SRM915b and BHVO-2 during this study yielded values consistent with those recommended in the literature (Table S-2).

2. Radiogenic Ca Isotope Variation in Pitcairn Lavas

The double spike technique used in this study allows the simultaneous, independent determination of $\delta^{44/40}$Ca and $\delta^{44/42}$Ca. Therefore, we can simultaneously get the sample's radiogenic Ca isotopic composition ($\varepsilon^{40/44}$Ca) using Eq. S-2 (He *et al.*, 2017). Overall, the Pitcairn lavas span $\varepsilon^{40/44}$Ca from −1.3 ± 0.5 to 0.4 ± 0.4 (typical analytical uncertainty ~ ±0.6 ε-units; Table S-1). The data separate systematically into two groups based on radiogenic Sr-Nd-Pb isotopic compositions (Fig. S-4a,b,c): (i) an EM1-like group comprising all Tedside samples + one seamount sample, with ^{87}Sr/^{86}Sr > 0.70448, ^{143}Nd/^{144}Nd < 0.512439, ^{206}Pb/^{204}Pb < 17.832, and a mean $\varepsilon^{40/44}$Ca = −0.1 ± 0.7 (2 s.d., n = 6), which is systematically higher than the BSE (from −1.2 to −0.6; Antonelli *et al.*, 2021; Wang *et al.*, 2024); and (ii) a more depleted/mid-ocean ridge basalt (MORB)-like group comprising six seamount samples + three post-erosional samples, averaging $\varepsilon^{40/44}$Ca = −0.8 ± 0.8 (2 s.d., n = 9), which is consistent with the BSE (Antonelli *et al.*, 2021; Wang *et al.*, 2024). A Student's t-test gives p = 0.006, indicating a statistically significant difference between the two groups (Fig. S-4d).

Given that seawater may strongly affect Sr isotopes but has only a weak influence on Nd isotopes (McCulloch *et al.*, 1981), the well-defined Sr-Nd isotopic coupling observed in the Pitcairn samples is unlikely to result from a single seawater-driven process and more likely reflects source-driven processes (*e.g.*, Woodhead *et al.*, 1993; Fig. S-1c). The EM1-like end member displays a higher radiogenic Ca isotope signature. Because of their low K/Ca (< 0.32) and young eruption ages (< 1 Ma) of Pitcairn lavas, any radiogenic ^{40}Ca growth over such timescales could be far below our analytical uncertainty. Thus, we consider post-eruptive in-situ ingrowth of ^{40}Ca to be negligible for the Tedside suite. Accordingly, the relatively higher $\varepsilon^{40/44}$Ca of Tedside samples compared with seamount samples most plausibly reflects source contributions from recycled materials, for example, carbonate-bearing recycled lithologies (and/or other enriched components), rather than seawater-driven processes.

Taken together, the radiogenic and stable Ca isotope data suggest that the contrasting behaviours of the Tedside and seamount lavas primarily reflect distinct lithologies in source. The seamount samples show mantle-like $\varepsilon^{40/44}$Ca but relatively light $\delta^{44/42}$Ca (Figs. S-2 and S-4), implying that their source contains only minor contributions from recycled surficial materials with $\varepsilon^{40/44}$Ca anomalies. Instead, their signatures are more consistent with a source dominated by recycled lower oceanic crust, whose incorporation into the ambient mantle forms secondary pyroxenite with lower $\delta^{44/42}$Ca, providing a plausible explanation for the lower $\delta^{44/42}$Ca of the seamount suite (Fig. 3). By contrast, the Tedside samples exhibit $\varepsilon^{40/44}$Ca slightly higher than the mantle (Fig. S-4), indicating a significant contribution from recycled surficial materials (*e.g.*, sedimentary carbonates), whereas their $\delta^{44/42}$Ca are close to MORB (Fig. S-2). This $\varepsilon^{40/44}$Ca-$\delta^{44/42}$Ca signature can be explained by two alternative scenarios: (i) the recycled carbonates entering the Pitcairn mantle source may have a relatively low Ca content. In that case, their large $\varepsilon^{40/44}$Ca difference may be sufficient to shift the bulk $\varepsilon^{40/44}$Ca of source, whereas any difference in their $\delta^{44/42}$Ca relative to the ambient mantle would have a negligible effect on the bulk $\delta^{44/42}$Ca to be resolved with our current analytical precision; and/or (ii) given the large and mantle-overlapping range of $\delta^{44/42}$Ca for sedimentary carbonates (Chen *et al.*, 2018), the recycled carbonate into the Pitcairn source may itself exhibit MORB-like $\delta^{44/42}$Ca, and therefore does not significantly shift the bulk $\delta^{44/42}$Ca of source. Future work will call on more high-precision stable and radiogenic Ca isotope data to further unravel the origin of Ca isotope variability in OIBs.

3. Modelling the Ca Isotope Composition of Melts in this Study

In this study, to explain the Ca isotope variation observed in Pitcairn basalts, we calculate the Ca isotopic composition of melts derived from the partial melting of eclogite, two types of secondary pyroxenite with varying garnet contents, garnet peridotite, and spinel peridotite. A non-modal batch melting model based on Williams and Bizimis (2014) is employed. The modelling results are summarised in Tables S-5 to S-10 below.

Firstly, we modelled the partial melting of spinel and garnet peridotite (Tables S-5 and S-6), as these two lithologies are considered representative of mantle sources without recycled components. However, the calculated trends of $\delta^{44/42}$Ca versus $(Dy/Yb)_N$ for these lithologies cannot explain the Pitcairn basalt data. For spinel peridotite (Table S-5), initial modal mode, melting mode, Ca partition coefficients (D_{Ca}), and bulk CaO content are taken from Workman and Hart (2005). Dy and Yb partition coefficients are from Salters and Stracke (2004). Contents of Dy and Yb are approximated as primitive mantle (Sun and McDonough, 1989). The initial $\delta^{44/42}$Ca of the mantle source is from Kang *et al.* (2017). Ca isotope fractionation factors between minerals and melt at 1000 K are taken from Antonelli *et al.* (2019) and Zhang *et al.* (2018), and then scaled to a magmatic temperature of 1673 K using a $1/T^2$ dependence (*i.e.* $\Delta^{44/42}Ca_{mineral\text{-}cpx}$ at

1673 K and $\Delta^{44/42}Ca_{melt\text{-}cpx}$ at 1673 K in Table S-5). These factors are widely accepted in the community for high-temperature Ca isotope modelling (*e.g.*, Soderman *et al.*, 2022). The calculated $\delta^{44/42}Ca$ of melt can be as low as 0.38 ‰ at very low degrees of melting, which clearly cannot account for the observed range in Pitcairn basalts (Fig. 3). We subsequently modelled the Ca isotopic composition of melts derived from garnet peridotite (Table S-6). Initial modal mode, melting mode, Ca partition coefficient, and bulk CaO are based on experimental studies of garnet peridotite melting (Davis *et al.*, 2011; Walter, 1998). Partition coefficients of Dy and Yb are taken from Salters *et al.* (2002). Contents of Dy and Yb, the $\delta^{44/42}Ca$ of mantle source, and Ca isotope fractionation factors are identical to those used in the spinel peridotite model (Sun and McDonough, 1989; Kang *et al.*, 2017; Zhang *et al.*, 2018; Antonelli *et al.*, 2019). The degree of melting ranges from 0 % to 22 % for spinel peridotite and from 0 % to 25 % for garnet peridotite, constrained by the near exhaustion of residual clinopyroxene. The lowest calculated $\delta^{44/42}Ca$ of the melt is 0.37 ‰, which still cannot reproduce the range observed in Pitcairn basalts (Fig. 3).

Next, we investigate high pressure eclogite-derived melts (referred to as HPEM in the main text), generated by the partial melting of recycled MORB at high pressure. The modelling procedure and results for HPEM are presented in Table S-7. The initial modal and melting modes are adopted from Sobolev *et al.* (2000), which simulate partial melting of eclogite derived from recycled crustal components at high pressure. Recycled oceanic crust transforms into silica-saturated eclogite under mantle P-T conditions, with high-pressure eclogites containing abundant garnet (Thomson *et al.*, 2016), facilitating the generation of Ca-isotopically light melts (Wang *et al.*, 2019). Mineral CaO contents and Ca partition coefficients between minerals and melt are based on the compositions of silicate melts and residual minerals obtained from high P-T experiments (3–5.1 GPa) on the partial melting of recycled MORB (Thomson *et al.*, 2016). Dy and Yb partition coefficients are from Sobolev *et al.* (2000). The bulk CaO content of the eclogite (10.06 wt. %) is calculated from modal mineralogy and partition coefficients, consistent with the average MORB value (11.39 wt. %; Arevalo and McDonough, 2010). Dy and Yb contents of the eclogite are from Arevalo and McDonough (2010), and its initial $\delta^{44/42}Ca$ is assumed to be the mean $\delta^{44/42}Ca$ of MORBs (Eriksen and Jacobsen, 2022). Ca isotope fractionation factors between minerals and melt are identical to those used for modelling peridotite melting (Antonelli *et al.*, 2019; Zhang *et al.*, 2018). We acknowledge that the calculated $\delta^{44/42}Ca$ of HPEM could be a maximum estimate, particularly if jadeite-rich clinopyroxene is also enriched in heavy Ca isotopes (Wang *et al.*, 2019). The degree of melting for recycled MORB ranges from 1 % to 34 %, until the exhaustion of residual coesite. These melts exhibit substantially light Ca isotope compositions due to abundant garnet proportion in the residue. However, the $(Dy/Yb)_N$ range of the HPEM is relatively narrow and does not fall within the range observed in Pitcairn basalts (Fig. 3).

We then consider a three-step model involving the formation and melting of secondary pyroxenites. Recycled oceanic crust is preferentially melted during mantle adiabatic upwelling (Ringwood and Green, 1966), and the resulting silica-

rich melts react with ambient peridotite to form secondary pyroxenite (Yaxley and Green, 1998; Sobolev *et al.*, 2000, 2005). Melting of secondary pyroxenite with abundant garnet in the residue can produce Ca-isotopically light melts (Wang *et al.*, 2019). Similar models have been widely applied to explain the origin of OIBs, including reproducing the trace element compositions of Pitcairn-Gambier OIBs (Delavault *et al.*, 2015), interpreting the characteristics of melt inclusions in Mauna Loa basalts with high Sr and low REE contents, and high Sr/Ce ratios (Sobolev *et al.*, 2000), as well as the high Ni and SiO_2 contents observed in Hawaiian shield-stage basalts (Sobolev *et al.*, 2005):

1. Generation of HPEM. As described above, recycled oceanic crust was modelled to undergo partial melting at ~30 %, producing eclogitic melts (Table S-7).

2. Formation of secondary pyroxenites. A binary mixing model is applied to estimate the trace element and Ca isotopic compositions of secondary pyroxenites (Table S-8). The recycled oceanic crust component is represented by the HPEM in Step 1, while the peridotite component is assumed to be depleted mantle (Salters and Stracke, 2004) with a Ca isotopic composition from Kang *et al.* (2017). Two scenarios are considered here: Secondary pyroxenite 1 comprises 5 % HPEM and 95 % peridotite, representing a garnet bearing lithology formed at relatively low pressure from upper oceanic crust-derived melts. The 5 % HPEM proportion is taken from the estimate obtained when evaluating the trace element compositions of the extreme EM-1 end member samples on Gambier Island in the Pitcairn chain (Delavault *et al.*, 2015), which suggests a source containing 5 % recycled oceanic crust and 95 % peridotite. Secondary pyroxenite 2 comprises 50 % HPEM and 50 % peridotite, representing a garnet-rich lithology formed at higher pressure from lower oceanic crust-derived melts. These assumptions are supported by mineral proportions observed in both modelling and experimental studies for reaction pyroxenites. Secondary pyroxenite formed by reaction between peridotite and melt derived from an eclogitised oceanic basalt at 3.5 GPa and 1350 °C contains 15.5 % garnet (Sobolev *et al.*, 2005), and experimental secondary pyroxenite formed at 3 GPa and 1475 °C contains ~10 % garnet (Tuff and Gibson, 2007). In contrast, secondary pyroxenite formed by reaction between peridotite and melt derived from eclogitised oceanic gabbro at 4.5 GPa and 1525 °C contains 24.3 % garnet (Sobolev *et al.*, 2005), and experimental secondary pyroxenite formed at 5 GPa and 1600 °C contains ~25 % garnet (Tuff and Gibson, 2007).

3. Partial melting of secondary pyroxenites. Melts derived from secondary pyroxenites 1 and 2 were modelled using a non-modal batch melting approach, with the results presented in Tables S-9 and S-10, respectively. The initial garnet proportion in secondary pyroxenite 1 is set at 10 %, and that in secondary pyroxenite 2 set at 24.3 % (Sobolev *et al.*, 2005; Tuff and Gibson, 2007), considering their distinct HPEM proportions. The melting mode follows Delavault *et al.* (2015). Ca partition coefficient is from Yaxley and Green (1998), and Dy and Yb partition

coefficients are from Pertermann *et al.* (2004). Bulk CaO, Dy, Yb contents and $\delta^{44/42}$Ca value are taken from Step 2 calculations. Ca isotope fractionation factors are the same as those used in Tables S-5 to S-7. The degree of melting ranges from 0 % to 21 % for secondary pyroxenite 1 and from 0 % to 50 % for secondary pyroxenite 2, constrained by the exhaustion of residual garnet.

The modelling results demonstrate that partial melting of secondary pyroxenite 2 can generate melts with $\delta^{44/42}$Ca values as low as those observed in the isotopically lightest Pitcairn basalts (Table S-10), and can effectively reproduce the $(Dy/Yb)_N$ variations of the Pitcairn samples (Fig. 3a). Meanwhile, melts derived from secondary pyroxenite 1 can also account for the MORB-like Ca isotope compositions observed in the Tedside samples. Given the extreme EM-1 end member trace element and radiogenic isotope characteristics of the Tedside lavas, we suggest that this pyroxenitic source is the primary contributor to their Ca isotope signatures, rather than a simple garnet peridotite source (Fig. 3a).

We further modelled the variations in stable Ca isotopic compositions and radiogenic isotopic ratios (*e.g.*, $^{87}Sr/^{86}Sr$) (Fig. 3b). To reproduce the enriched $^{87}Sr/^{86}Sr$ of Tedside lavas, carbonate bearing sediments were added to the source of HPEM (*i.e.* recycled oceanic crust). Firstly, a simple binary mixing approach was used to evaluate the effect of sediment addition. Carbonate-bearing sediments were added to recycled oceanic crust to generate the HPEM component. The recycled oceanic crust was assumed to have Sr = 130 ppm, CaO = 11.4 wt. %, $^{87}Sr/^{86}Sr$ = 0.704250 (White and Klein, 2014), and $\delta^{44/42}$Ca = 0.39 ‰ (Eriksen and Jacobsen, 2022). The carbonate-bearing sediment component was assumed to have CaO = 40 wt. % with $\delta^{44/42}$Ca = 0.29 ‰, and Sr = 1151 ppm with $^{87}Sr/^{86}Sr$ = 0.70880 (Fantle and Tipper, 2014; Huang and Xiao, 2016). The calcium carbonate composition is adopted here to approach the scenario, in which Ca isotope systematics of the hybridised source might have been influenced the most by addition of sediments. Based on the Ca isotope fractionation associated with high-pressure melting of recycled oceanic crust (~0.07 ‰; Table S-7), and assuming that $^{87}Sr/^{86}Sr$ remain unchanged during partial melting, we calculated the variations in $\delta^{44/42}$Ca and $^{87}Sr/^{86}Sr$ for melts derived from mixtures of recycled oceanic crust and carbonate-bearing sediments. The results are illustrated by the blue dashed line in Figure 3b. Because carbonate-bearing sediments have much higher Sr concentrations and higher $^{87}Sr/^{86}Sr$ than oceanic crust, the addition of small amounts of sediment significantly shifts the $^{87}Sr/^{86}Sr$ of the melt. In contrast, the effect on $\delta^{44/42}$Ca is limited due to relatively smaller difference in CaO contents and Ca isotopic compositions between sediments and oceanic crust. For example, the addition of 5 % carbonate-bearing sediments lowers the melt $\delta^{44/42}$Ca by only ~0.02 ‰ (Fig. 3b), which is much smaller than the Ca isotope fractionation generated during partial melting of recycled oceanic crust (~0.07 ‰, Table S-7).

We then modelled the formation of secondary pyroxenites through interaction between HPEM and ambient mantle peridotite using the same binary mixing approach as applied in Figure 3a. The mantle peridotite was assumed to contain

10 ppm Sr with $^{87}Sr/^{86}Sr$ = 0.70330 (Sobolev *et al.*, 2005), and 3.55 wt. % CaO with $\delta^{44/42}Ca$ = 0.42 ‰ (Kang *et al.*, 2017). The HPEM was assumed to contain 300 ppm Sr with $^{87}Sr/^{86}Sr$ = 0.70425 (Sobolev *et al.*, 2005), and 11.4 wt. % CaO with $\delta^{44/42}Ca$ = 0.32 ‰ corresponding to the HPEM composition estimated in this study (Table S-7). Specifically, to reproduce the enriched $^{87}Sr/^{86}Sr$ of the Tedside lavas, 5 % carbonate-bearing sediments were added to recycled oceanic crust to generate HPEM containing 5 % sediments. The Sr and Ca isotopic compositions of this HPEM component were taken from the calculation described above (blue dashed line in Fig. 3b). The calculated mixing relationships between HPEM and mantle peridotite are shown as two grey dashed lines in Figure 3b. Secondary pyroxenite 1 was generated from 5 % HPEM (with 5 % sediment added to its source) + 95 % ambient peridotite, whereas secondary pyroxenite 2 was generated from 50 % HPEM + 50 % ambient peridotite, consistent with the calculation in Figure 3a (*i.e.* the grey dashed line in Fig. 3a). The presence or absence of sediment components is consistent with the general understanding of how sediments are carried by subducting oceanic crust, with the upper oceanic crust typically incorporating more sediments than the lower crust. Partial melting of these secondary pyroxenites (illustrated by white arrows in Fig. 3b) can reproduce the observed Ca isotope variations in Pitcairn lavas (Fig. 3b). These results suggest that the Ca isotope variations are primarily controlled by the proportion of recycled oceanic crust-derived HPEM in the Pitcairn mantle plume and by Ca isotope fractionation associated with subsequent partial melting. In contrast, the addition of carbonate-bearing sediments is mainly required to reproduce the enriched radiogenic isotope signatures of the EM-1 component and has only a limited effect on Ca isotopes, consistent with the observation that the most enriched samples display MORB-like $\delta^{44/42}Ca$ values.

The $\delta^{44/42}Ca$ range observed in Pitcairn basalts in this study is broadly consistent with global OIBs, and their REE compositions are comparable to those of the isotopically lightest OIB samples from other hotspots (Eriksen *et al.*, 2024; Eriksen and Jacobsen, 2022). Notably, OIB samples with the highest $(Dy/Yb)_N$ do not exhibit the lightest Ca isotope compositions. Although the mechanism by which recycled oceanic crust components influence Ca isotopic compositions in OIBs from other hotspots remains unclear, the secondary pyroxenite partial melting model proposed in this study may offer a new explanation for the observed relationship between $\delta^{44/42}Ca$ and $(Dy/Yb)_N$ in global OIBs. According to our model, partial melting of secondary pyroxenites with variable garnet proportions can account for the variations observed in $\delta^{44/42}Ca$ versus $(Dy/Yb)_N$ (Fig. 4). Here, the composition of secondary pyroxenite is modelled as a binary mixing between mantle peridotite and HPEM in varying proportions. As shown by the black grid in Figure 4, vertical lines represent the proportion of HPEM involved in secondary pyroxenite formation (ranging from 0 % to 100 %), with the remaining proportion being mantle peridotite. Horizontal lines represent the degree of partial melting of the secondary pyroxenite (from 20 % to 60 %). Given that secondary pyroxenites formed from different proportions of HPEM are expected to have distinct modal abundances of garnet and clinopyroxene, they may therefore undergo melting under different conditions. Nevertheless, for the sake of model simplicity and comparability, we adopted the same

melting parameters as those used in Figure 3 and Tables S-9 and S-10. The results show that secondary pyroxenites formed from high proportions of HPEM (*i.e.* with higher garnet proportions) undergoing varying degrees of partial melting reproduce the Ca isotope variation observed in OIBs (Fig. 4). Given that previous studies have demonstrated significant contributions of secondary pyroxenite in some hotspot magmas (*e.g.*, >80 % in Koolau, Hawaii; Sobolev *et al.*, 2005), partial melting of secondary pyroxenites may provide a new perspective for interpreting Ca isotope anomalies at other hotspots.

Supplementary Tables

Tables S-1 to S-10 (.xlsx) are available for download from the online version of this article at https://doi.org/10.7185/geochemlet.2613

Table S-1 Calcium isotopic compositions for Pitcairn Island and seamount basalts.

a. 2 s.e. denotes two standard errors of the mean, 2 s.e. = 2s.d./sqrt(n).

b. $\varepsilon^{40/44}$Ca is calculated from independently obtained $\delta^{44/42}$Ca and $\delta^{44/40}$Ca, following the method of Farkaš *et al.* (2011).

c. n denotes number of analyses of Ca isotopes.

Table S-2 Calcium isotopic compositions of standard materials.

a. Reference sources: Zhu *et al.* (2020); Dai *et al.* (2022); Eriksen and Jacobsen (2022).

b. 2 s.d. denotes two standard deviations.

c. n denotes number of analyses of Ca isotopes.

Table S-3 Major and trace element concentrations for Pitcairn Island and seamount basalts. Major and trace element concentration data are from Woodhead and McCulloch (1989) and Woodhead and Devey (1993).

Table S-4 Trace element concentrations corrected for the olivine accumulation for Pitcairn Island and seamount basalts. Trace element concentrations (Woodhead and McCulloch, 1989; Woodhead and Devey, 1993) are corrected for the olivine accumulation to 9.5 wt. % MgO. Three evolved samples with MgO < 3.8 wt. % (denoted by *) were excluded from this correction. Partition coefficients used in the correction are from Bédard (2005).

Table S-5 Calcium isotopic compositions of spinel peridotite melt.

Parameters sources: a. Workman and Hart (2005); b. Salters and Stracke (2004); c. Antonelli *et al.* (2019); d. Zhang *et al.* (2018); e. Sun and McDonough (1989); f. Kang *et al.* (2017). g. The subscript N denotes normalisation of residual phases to 100 %.

Table S-6 Calcium isotopic compositions of garnet peridotite melt.

Parameters sources: a. Davis et al. (2011); b. Walter (1998); c. Salters and Stracke (2004); d. Antonelli *et al.* (2019); e. Zhang *et al.* (2018); f. Sun and McDonough (1989); g. Kang *et al.* (2017). h. The subscript N denotes normalisation of residual phases to 100 %.

Table S-7 Calcium isotopic compositions of high pressure eclogite-derived melt (HPEM).

Parameters sources: a. Sobolev *et al.* (2000); b. Thomson *et al.* (2016); c. Antonelli *et al.* (2019); d. Zhang *et al.* (2018); e. Arevalo and McDonough (2010); f. Eriksen and Jacobsen (2022). g. The subscript N denotes normalisation of residual phases to 100 %.

Table S-8 Formation models for two types of secondary pyroxenite.

a. HPEM = high pressure eclogite-derived melt, and its composition corresponds to the 30 % partial melting result in Table S-7.

b. PM = primitive mantle (Sun and McDonough, 1989).

Table S-9 Calcium isotopic compositions of melt from secondary pyroxenite 1.

Parameters sources: a. Sobolev *et al.* (2005); b. Delavault *et al.* (2015); c. Table S-8; d. Yaxley and Green (1998); e. Pertermann *et al.* (2004); f. Antonelli *et al.* (2019); g. Zhang *et al.* (2018). h. The subscript N denotes normalisation of residual phases to 100 %.

Table S-10 Calcium isotopic compositions of melt from secondary pyroxenite 2.

Parameters sources: a. Sobolev *et al.* (2005); b. Delavault *et al.* (2015); c. Table S-8; d. Yaxley and Green (1998); e. Pertermann *et al.* (2004); f. Antonelli *et al.* (2019); g. Zhang *et al.* (2018). h. The subscript N denotes normalisation of residual phases to 100 %.

Supplementary Figures

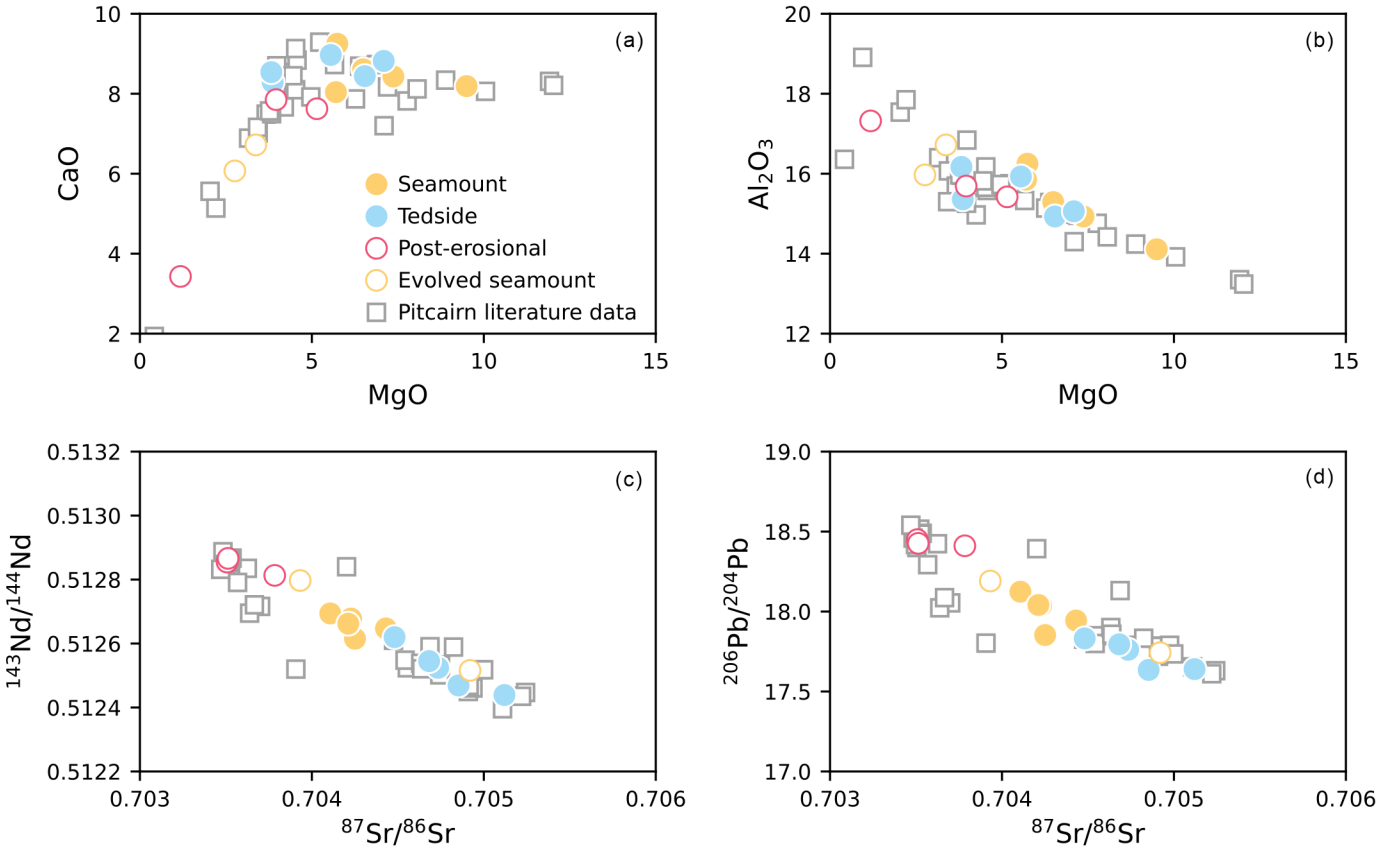

Figure S-1 **(a)** CaO *vs.* MgO, **(b)** Al_2O_3 *vs.* MgO, **(c)** $^{143}Nd/^{144}Nd$ *vs.* $^{87}Sr/^{86}Sr$, **(d)** $^{206}Pb/^{204}Pb$ *vs.* $^{87}Sr/^{86}Sr$ for Pitcairn basalts. Pitcairn basalt data are taken from the GEOROC database (http://georoc.eu/).

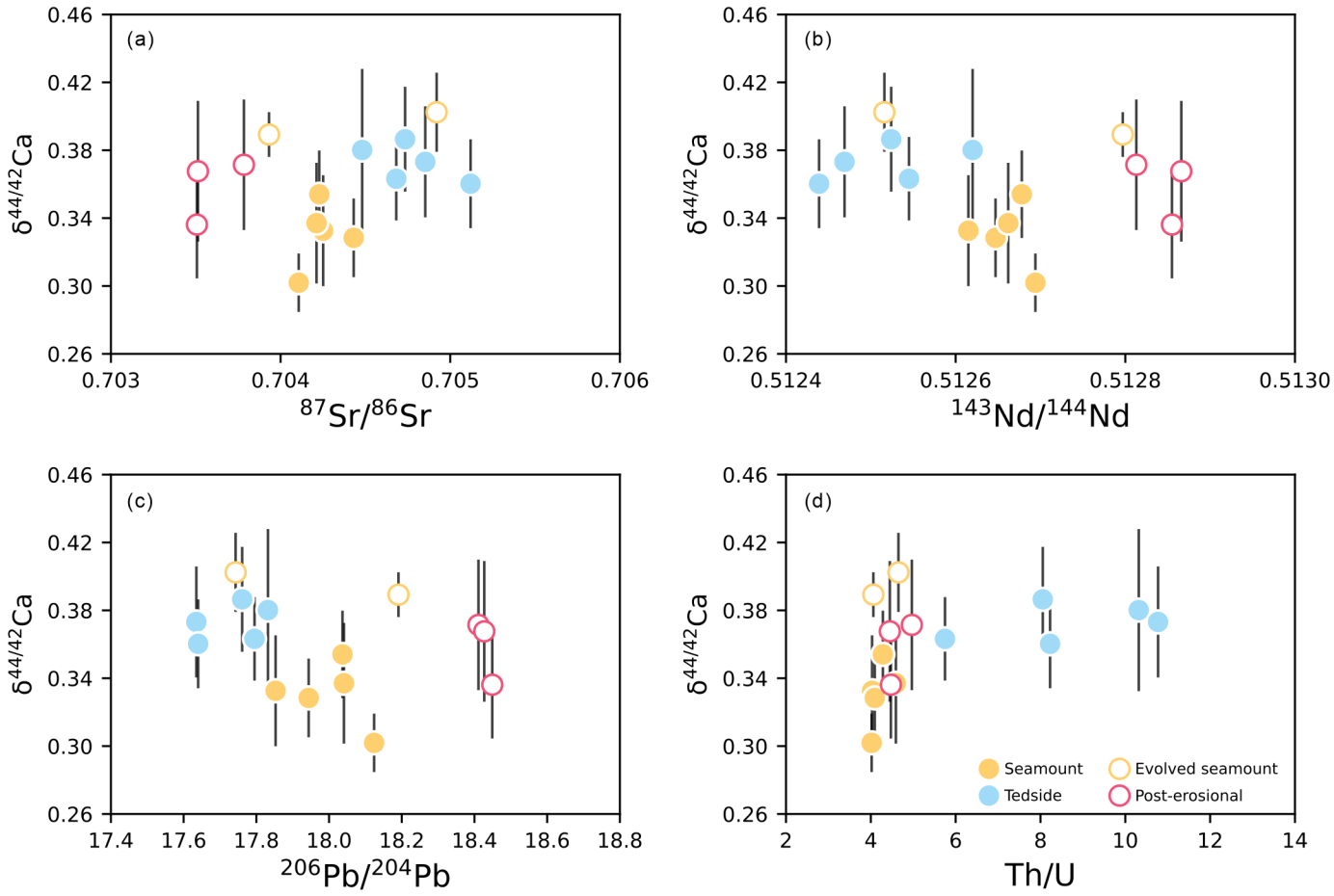

Figure S-2 $\delta^{44/42}$Ca *vs.* **(a)** ^{87}Sr/^{86}Sr, **(b)** ^{143}Nd/^{144}Nd, **(c)** ^{206}Pb/^{204}Pb and **(d)** Th/U for Pitcairn basalts. Typical 2 s.e. for $\varepsilon^{40/44}$Ca and $\delta^{44/42}$Ca are ±0.03 ‰ and ±0.6 ε, respectively. Hollow symbols denote evolved samples with MgO < 3.8 wt. %. Trace elemental and isotopic data are from Woodhead and McCulloch (1989) and Woodhead and Devey (1993). Trace element data for Pitcairn basalts were corrected for the influence of olivine accumulation, following Nebel *et al.* (2019), except for samples with MgO < 3.8 wt. % due to the unavailability of an effective correction method for clinopyroxene fractionation.

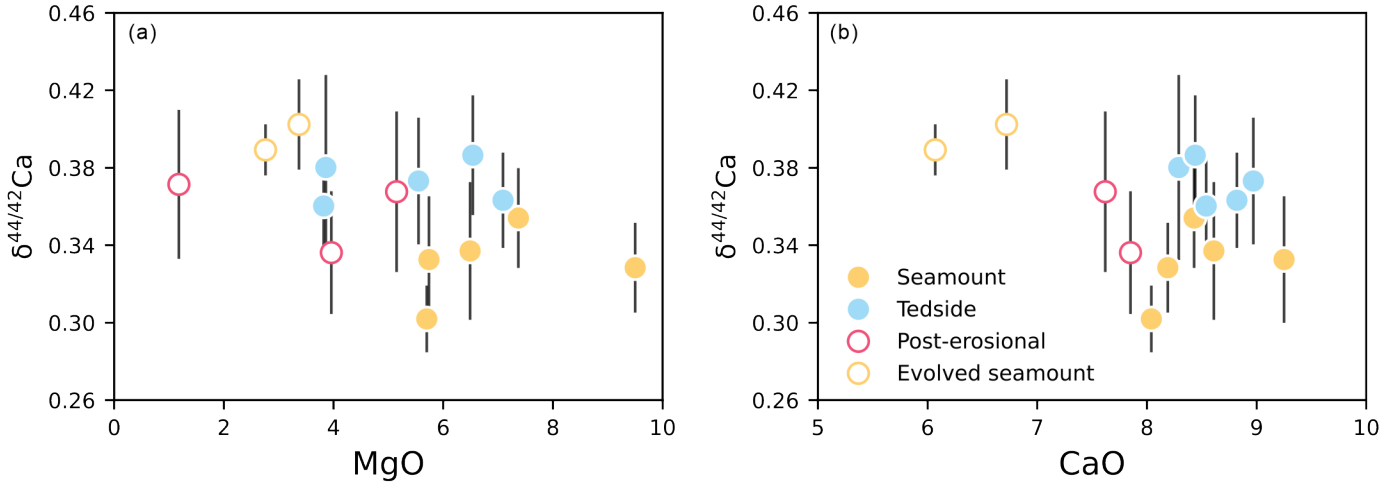

Figure S-3 $\delta^{44/42}$Ca *vs.* **(a)** MgO and **(b)** CaO for Pitcairn basalts.

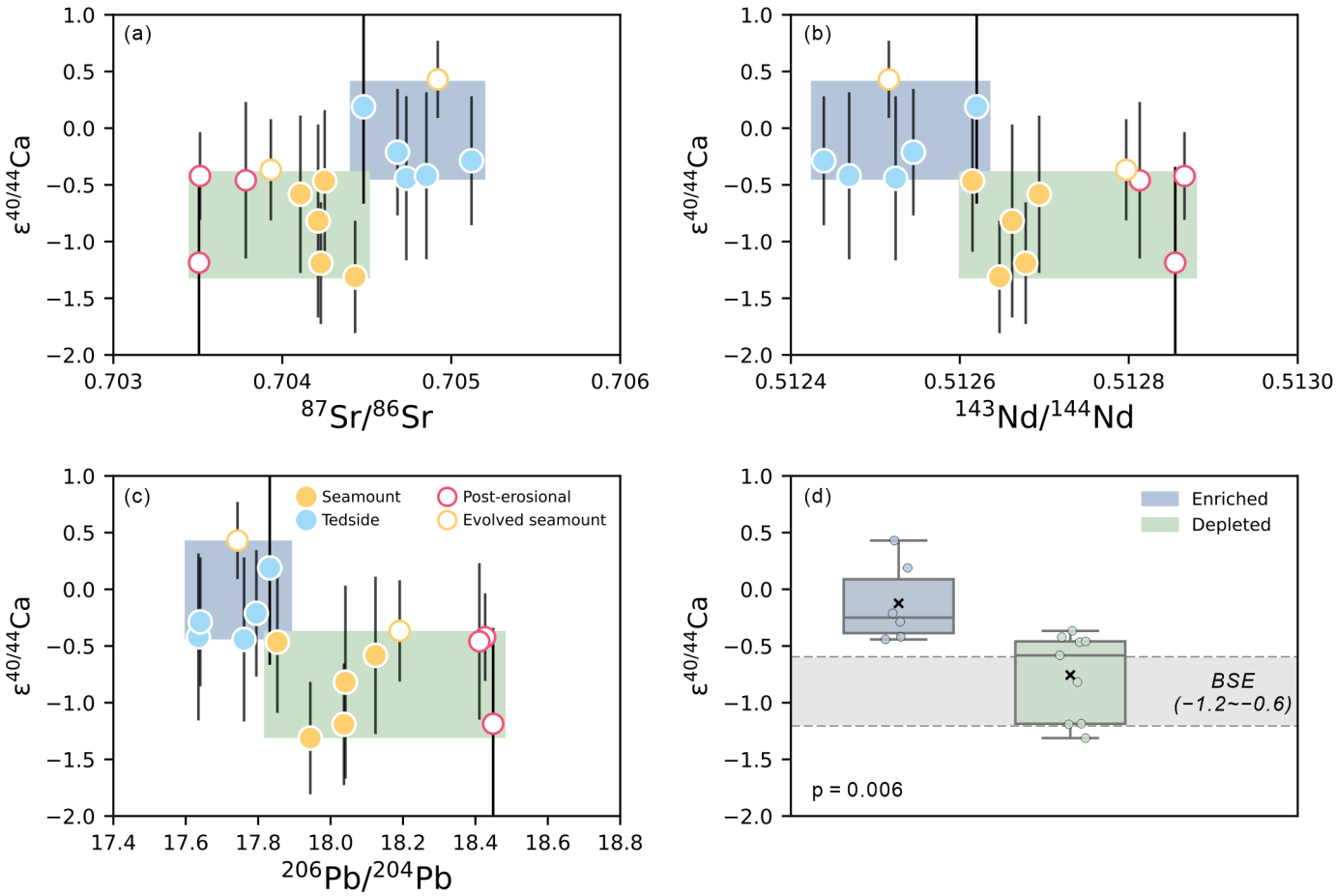

Figure S-4 $\varepsilon^{40/44}$Ca *vs.* **(a)** $^{87}Sr/^{86}Sr$, **(b)** $^{143}Nd/^{144}Nd$, and **(c)** $^{206}Pb/^{204}Pb$ for Pitcairn lavas, and **(d)** a two-sample t-test

for relatively enriched and depleted groups of Pitcairn lavas, which gives p = 0.006, indicating a significant difference between the enriched and depleted groups.

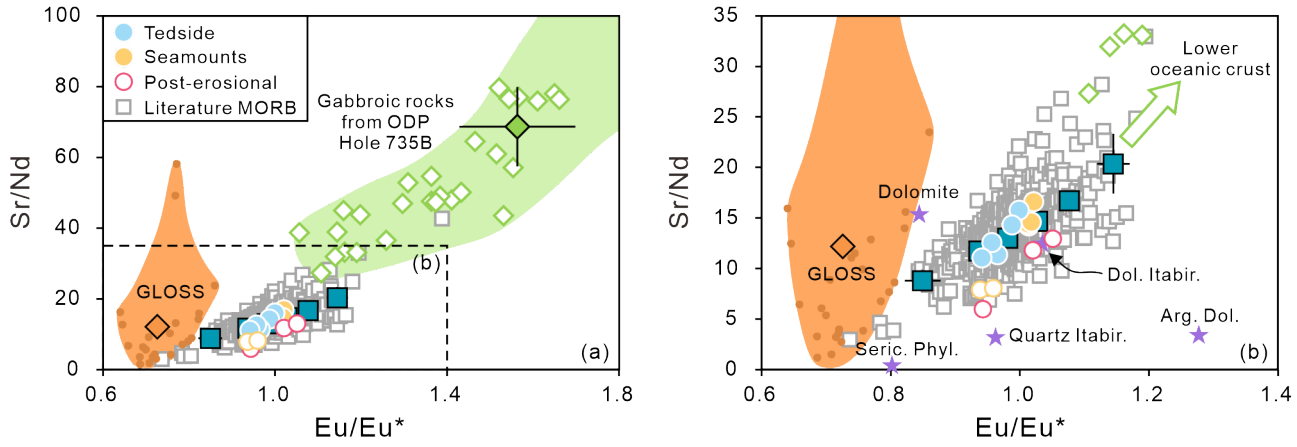

Figure S-5 Sr/Nd *vs.* Eu/Eu* for Pitcairn basalts, with MORB, GLOSS, and gabbroic rock data for comparison. MORB data are from Arevalo and McDonough (2010). The data have been categorised into six groups based on Eu/Eu* values: ≤ 0.90, 0.90–0.95, *etc*. Grey squares denote mean values of MORB corresponding to six segments of data based on Eu/Eu*. The orange region represents the sediment columns subducting at different trenches, with the orange rhombus indicating the mean GLOSS composition (Plank and Langmuir, 1998). Green hollow rhombuses represent gabbroic rocks from ODP Hole 735B (Bach *et al.*, 2001), and the green solid symbol indicates the mean value of these gabbroic rocks, representing lower oceanic crust. Purple pentagrams in panel (b) indicate possible terrestrial and marine sediment components (Spier *et al.*, 2007). Abbreviations: Seric. Phyl. — Sericitic phyllite; Arg. Dol. — Argillaceous dolomite; Dol. Itabir. — Dolomitic itabirite; Quartz Itabir. — Quartz itabirite.

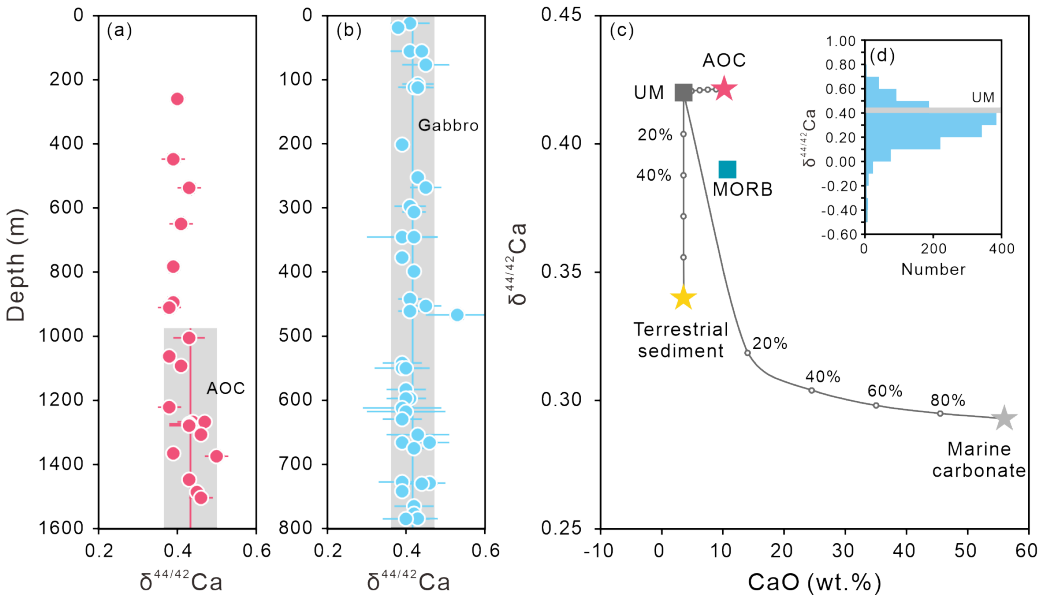

Figure S-6 **(a)** $\delta^{44/42}$Ca for altered oceanic crustal rocks, **(b)** $\delta^{44/42}$Ca for gabbros, **(c)** mixing lines between the upper mantle and different recycled materials, and **(d)** $\delta^{44/42}$Ca for marine carbonates. Altered oceanic crust and gabbro samples are from IODP Site 1256 and Hole U1473A, respectively. Sources for $\delta^{44/42}$Ca of end members in panel (c): AOC—the mean value for altered oceanic crustal rocks; terrestrial sediment—assumed to be equivalent to the upper continental crust; marine carbonates—the mean value based on previously reported data (Fantle and Tipper, 2014).

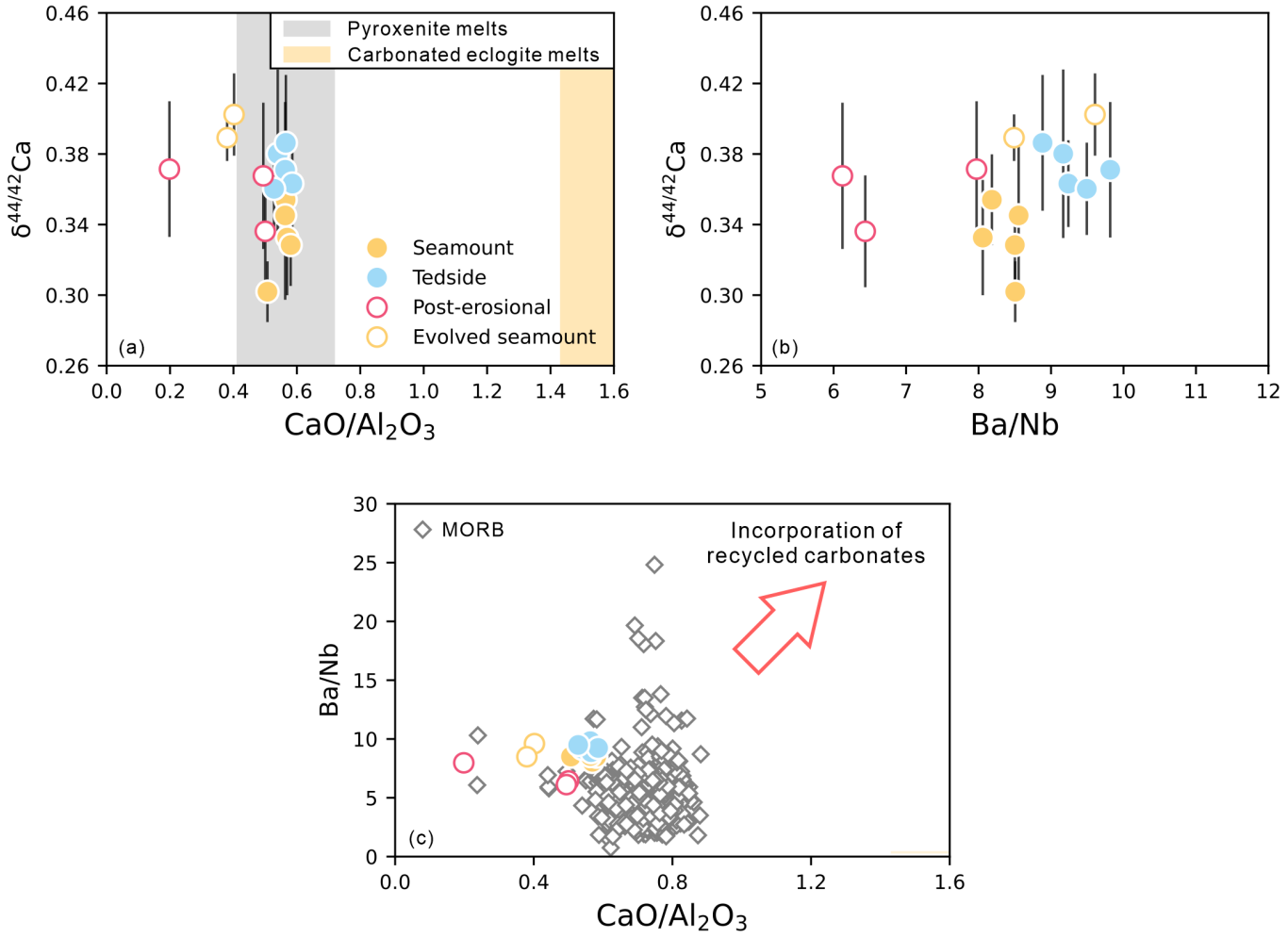

Figure S-7 (a) $\delta^{44/42}$Ca *vs.* CaO/Al_2O_3, **(b)** $\delta^{44/42}$Ca *vs.* Ba/Nb, and **(c)** Ba/Nb *vs.* CaO/Al_2O_3. Grey and yellow shaded regions in panel (a) represent experimental pyroxenite melts (Pertermann and Hirschmann, 2003) and carbonated eclogite melts (Dasgupta *et al.*, 2006), respectively. Hollow diamonds in panel (c) represent literature MORB data (Arevalo and McDonough, 2010).

Supplementary Information References

Antonelli, M.A., DePaolo, D.J., Christensen, J.N., Wotzlaw, J.-F., Pester, N.J., Bachmann, O. (2021) Radiogenic ^{40}Ca in Seawater: Implications for Modern and Ancient Ca Cycles. *ACS Earth and Space Chemistry* 5, 2481–2492. https://doi.org/10.1021/acsearthspacechem.1c00179

Antonelli, M.A., Schiller, M., Schauble, E.A., Mittal, T., DePaolo, D.J., Chacko, T., Grew, E.S., Tripoli, B. (2019) Kinetic and equilibrium Ca isotope effects in high-T rocks and minerals. *Earth and Planetary Science Letters* 517, 71–82. https://doi.org/10.1016/j.epsl.2019.04.013

Arevalo, R., McDonough, W.F. (2010) Chemical variations and regional diversity observed in MORB. *Chemical Geology* 271, 70–85. https://doi.org/10.1016/j.chemgeo.2009.12.013

Bach, W., Alt, J.C., Niu, Y., Humphris, S.E., Erzinger, J., Dick, H.J.B. (2001) The geochemical consequences of late-stage low-grade alteration of lower ocean crust at the SW Indian Ridge: results from ODP Hole 735B (Leg 176). *Geochimica et Cosmochimica Acta* 65, 3267–3287. https://doi.org/10.1016/S0016-7037(01)00677-9

Bédard, J.H. (2005) Partitioning coefficients between olivine and silicate melts. *Lithos* 83, 394–419. https://doi.org/10.1016/j.lithos.2005.03.011

Chen, C., Liu, Y., Feng, L., Foley, S.F., Zhou, L., Ducea, M.N., Hu, Z. (2018) Calcium isotope evidence for subduction-enriched lithospheric mantle under the northern North China Craton. *Geochimica et Cosmochimica Acta* 238, 55–67. https://doi.org/10.1016/j.gca.2018.06.038

Dai, W., Moynier, F., Paquet, M., Moureau, J., Debret, B., Siebert, J., Gerard, Y., Zhao, Y. (2022) Calcium isotope measurements using a collision cell (CC)-MC-ICP-MS. *Chemical Geology* 590, 120688. https://doi.org/10.1016/j.chemgeo.2021.120688

Dasgupta, R., Hirschmann, M.M., Stalker, K. (2006) Immiscible Transition from Carbonate-rich to Silicate-rich Melts in the 3 GPa Melting Interval of Eclogite + CO_2 and Genesis of Silica-undersaturated Ocean Island Lavas. *Journal of Petrology* 47, 647–671. https://doi.org/10.1093/petrology/egi088

Davis, F.A., Hirschmann, M.M., Humayun, M. (2011) The composition of the incipient partial melt of garnet peridotite at 3 GPa and the origin of OIB. *Earth and Planetary Science Letters* 308, 380–390. https://doi.org/10.1016/j.epsl.2011.06.008

Delavault, H., Chauvel, C., Sobolev, A., Batanova, V. (2015) Combined petrological, geochemical and isotopic modeling of a plume source: Example of Gambier Island, Pitcairn chain. *Earth and Planetary Science Letters* 426, 23–35. https://doi.org/10.1016/j.epsl.2015.06.013

Delavault, H., Chauvel, C., Thomassot, E., Devey, C.W., Dazas, B. (2016) Sulfur and lead isotopic evidence of relic Archean sediments in the Pitcairn mantle plume. *Proceedings of the National Academy of Sciences* 113, 12952–12956. https://doi.org/10.1073/pnas.1523805113

Eriksen, Z.T., Jacobsen, S.B. (2022) Calcium isotope constraints on OIB and MORB petrogenesis: The importance of melt mixing. *Earth and Planetary Science Letters* 593, 117665. https://doi.org/10.1016/j.epsl.2022.117665

Eriksen, Z.T., Jacobsen, S.B., Day, J.M.D., White, W.M. (2024) Calcium isotope variability among ocean islands reveals the physical and lithological controls on mantle partial melting. *Geochimica et Cosmochimica Acta*. https://doi.org/10.1016/j.gca.2024.02.011

Fantle, M.S., Tipper, E.T. (2014) Calcium isotopes in the global biogeochemical Ca cycle: Implications for development of a Ca isotope proxy. *Earth-Science Reviews* 129, 148–177. https://doi.org/10.1016/j.earscirev.2013.10.004

Farkaš, J., Déjeant, A., Novák, M., Jacobsen, S.B. (2011) Calcium isotope constraints on the uptake and sources of Ca^{2+} in a base-poor forest: A new concept of combining stable ($\delta^{44/42}Ca$) and radiogenic (εCa) signals. *Geochimica et Cosmochimica Acta* 75, 7031–7046. https://doi.org/10.1016/j.gca.2011.09.021

He, Y., Wang, Y., Zhu, C., Huang, S., Li, S. (2017) Mass-Independent and Mass-Dependent Ca Isotopic Compositions of Thirteen Geological Reference Materials Measured by Thermal Ionisation Mass Spectrometry. *Geostandards and Geoanalytical Research* 41, 283–302. https://doi.org/10.1111/ggr.12153

Huang, J., Xiao, Y. (2016) Mg-Sr isotopes of low-$\delta^{26}Mg$ basalts tracing recycled carbonate species: Implication for the initial melting depth of the carbonated mantle in Eastern China. *International Geology Review* 58, 1350–1362. https://doi.org/10.1080/00206814.2016.1157709

Kang, J.-T., Ionov, D.A., Liu, F., Zhang, C.-L., Golovin, A.V., Qin, L.-P., Zhang, Z.-F., Huang, F. (2017) Calcium isotopic fractionation in mantle peridotites by melting and metasomatism and Ca isotope composition of the Bulk Silicate Earth. *Earth and Planetary Science Letters* 474, 128–137. https://doi.org/10.1016/j.epsl.2017.05.035

McCulloch, M.T., Gregory, R.T., Wasserburg, G.J., Taylor, H.P. (1981) Sm-Nd, Rb-Sr, and^{18} O/^{16} O isotopic systematics in an oceanic crustal section: Evidence from the Samail Ophiolite. *Journal of Geophysical Research: Solid Earth* 86, 2721–2735. https://doi.org/10.1029/JB086iB04p02721

Nebel, O., Sossi, P.A., Bénard, A., Arculus, R.J., Yaxley, G.M., Woodhead, J.D., Rhodri Davies, D., Ruttor, S. (2019) Reconciling petrological and isotopic mixing mechanisms in the Pitcairn mantle plume using stable Fe isotopes. *Earth and Planetary Science Letters* 521, 60–67. https://doi.org/10.1016/j.epsl.2019.05.037

Pertermann, M., Hirschmann, M.M. (2003) Anhydrous Partial Melting Experiments on MORB-like Eclogite: Phase Relations, Phase Compositions and Mineral-Melt Partitioning of Major Elements at 2-3 GPa. *Journal of Petrology* 44, 2173–2201. https://doi.org/10.1093/petrology/egg074

Pertermann, M., Hirschmann, M.M., Hametner, K., Günther, D., Schmidt, M.W. (2004) Experimental determination of trace element partitioning between garnet and silica-rich liquid during anhydrous partial melting of MORB-like eclogite. *Geochemistry, Geophysics, Geosystems* 5, 2003GC000638. https://doi.org/10.1029/2003GC000638

Plank, T., Langmuir, C.H. (1998) The chemical composition of subducting sediment and its consequences for the crust and mantle. *Chemical Geology* 145, 325–394. https://doi.org/10.1016/S0009-2541(97)00150-2

Ringwood, A.E., Green, D.H. (1966) An experimental investigation of the Gabbro-Eclogite transformation and some geophysical implications. *Tectonophysics* 3, 383–427. https://doi.org/10.1016/0040-1951(66)90009-6

Salters, V.J.M., Longhi, J.E., Bizimis, M. (2002) Near mantle solidus trace element partitioning at pressures up to 3.4 GPa. *Geochemistry, Geophysics, Geosystems* 3, 1–23. https://doi.org/10.1029/2001GC000148

Salters, V.J.M., Stracke, A. (2004) Composition of the depleted mantle. *Geochemistry, Geophysics, Geosystems* 5, 2003GC000597. https://doi.org/10.1029/2003GC000597

Sobolev, A.V., Hofmann, A.W., Nikogosian, I.K. (2000) Recycled oceanic crust observed in 'ghost plagioclase' within the source of Mauna Loa lavas. *Nature* 404, 986–990. https://doi.org/10.1038/35010098

Sobolev, A.V., Hofmann, A.W., Sobolev, S.V., Nikogosian, I.K. (2005) An olivine-free mantle source of Hawaiian shield basalts. *Nature* 434, 590–597. https://doi.org/10.1038/nature03411

Soderman, C.R., Shorttle, O., Matthews, S., Williams, H.M. (2022) Global trends in novel stable isotopes in basalts: Theory and observations. *Geochimica et Cosmochimica Acta* 318, 388–414. https://doi.org/10.1016/j.gca.2021.12.008

Spier, C., Deoliveira, S., Sial, A., Rios, F. (2007) Geochemistry and genesis of the banded iron formations of the Cauê Formation, Quadrilátero Ferrífero, Minas Gerais, Brazil. *Precambrian Research* 152, 170–206. https://doi.org/10.1016/j.precamres.2006.10.003

Sun, S.-s., McDonough, W.F. (1989) Chemical and isotopic systematics of oceanic basalts: implications for mantle composition and processes. *Geological Society, London, Special Publications* 42, 313–345. https://doi.org/10.1144/GSL.SP.1989.042.01.19

Thomson, A.R., Walter, M.J., Kohn, S.C., Brooker, R.A. (2016) Slab melting as a barrier to deep carbon subduction. *Nature* 529, 76–79. https://doi.org/10.1038/nature16174

Tuff, J., Gibson, S.A. (2007) Trace-element partitioning between garnet, clinopyroxene and Fe-rich picritic melts at 3 to 7 GPa. *Contributions to Mineralogy and Petrology* 153, 369–387. https://doi.org/10.1007/s00410-006-0152-x

Walter, M.J. (1998) Melting of Garnet Peridotite and the Origin of Komatiite and Depleted Lithosphere. *Journal of Petrology* 39, 29–60. https://doi.org/10.1093/petroj/39.1.29

Wang, Y., He, Y., Wang, Z.-N., Lu, W.-N., Meng, X.-N., Zhu, C., Ke, S. (2023) High-Precision Calcium Isotope Analysis on TIMS Using A Double Spike Technique: The Instrumental Drift and Its Correction. *Atomic Spectroscopy* 44, 45–54. https://doi.org/10.46770/AS.2023.043

Wang, Y., He, Y., Wu, H., Zhu, C., Huang, S., Huang, J. (2019) Calcium isotope fractionation during crustal melting and magma differentiation: Granitoid and mineral-pair perspectives. *Geochimica et Cosmochimica Acta* 259, 37–52. https://doi.org/10.1016/j.gca.2019.05.030

Wang, Z.-N., Wang, Y., Sossi, P., He, Y., Peng, Y., Lu, W.-N., Wu, H. (2024) Calcium isotopic composition of the bulk silicate Earth: A komatiite perspective. *Lithos* 480–481, 107638. https://doi.org/10.1016/j.lithos.2024.107638

White, W.M., Klein, E.M. (2014) 4.13 - Composition of the Oceanic Crust. *Treatise on Geochemistry*. Elsevier, 457–496. https://doi.org/10.1016/B978-0-08-095975-7.00315-6

Williams, H.M., Bizimis, M. (2014) Iron isotope tracing of mantle heterogeneity within the source regions of oceanic basalts. *Earth and Planetary Science Letters* 404, 396–407. https://doi.org/10.1016/j.epsl.2014.07.033

Woodhead, J.D., Devey, C.W. (1993) Geochemistry of the Pitcairn seamounts, I: source character and temporal trends. *Earth and Planetary Science Letters* 116, 81–99. https://doi.org/10.1016/0012-821X(93)90046-C

Woodhead, J.D., Greenwood, P., Harmon, R.S., Stoffers, P. (1993) Oxygen isotope evidence for recycled crust in the source of EM-type ocean island basalts. *Nature* 362, 809–813. https://doi.org/10.1038/362809a0

Woodhead, J.D., McCulloch, M.T. (1989) Ancient seafloor signals in Pitcairn Island lavas and evidence for large amplitude, small length-scale mantle heterogeneities. *Earth and Planetary Science Letters* 94, 257–273. https://doi.org/10.1016/0012-821X(89)90145-3

Workman, R.K., Hart, S.R. (2005) Major and trace element composition of the depleted MORB mantle (DMM). *Earth and Planetary Science Letters* 231, 53–72. https://doi.org/10.1016/j.epsl.2004.12.005

Yaxley, G.M., Green, D.H. (1998) Reactions between eclogite and peridotite: Mantle refertilisation by subduction of oceanic crust. *Schweizerische mineralogische und petrographische Mitteilungen* 78, 243–255. petrographische Mitteilungen 78, 243-255.

Zhang, H., Wang, Y., He, Y., Teng, F., Jacobsen, S.B., Helz, R.T., Marsh, B.D., Huang, S. (2018) No Measurable Calcium Isotopic Fractionation During Crystallization of Kilauea Iki Lava Lake. *Geochemistry, Geophysics, Geosystems* 19, 3128–3139. https://doi.org/10.1029/2018GC007506

Zhu, H., Liu, F., Li, X., An, Y., Nan, X., Du, L., Huang, F., Sun, W., Zhang, Z. (2020) Significant $\delta^{44/40}$Ca variations between carbonate- and clay-rich marine sediments from the Lesser Antilles forearc and implications for mantle heterogeneity. *Geochimica et Cosmochimica Acta* 276, 239–257. https://doi.org/10.1016/j.gca.2020.02.033